

Editors:  
Giorgio Ambrosio (FNAL)  
Paolo Ferracin (CERN)



FERMILAB-TM-2660-TD  
LARP Note  
US-HiLumi DocDB 186  
July 7, 2016

## MQXFS1 QUADRUPOLE FABRICATION REPORT

G. Ambrosio<sup>1</sup>, M. Anerella<sup>2</sup>, R. Bossert<sup>1</sup>, E. Cavanna<sup>4</sup>, D. Cheng<sup>3</sup>, G. Chlachidize<sup>1</sup>, L. Cooley<sup>1</sup>,  
D. Dietderich<sup>3</sup>, H. Felice<sup>3</sup>, P. Ferracin<sup>4</sup>, A. Ghosh<sup>2</sup>, R. Hafalia<sup>3</sup>, E.F. Holik<sup>1</sup>,  
S. Izquierdo Bermudez<sup>4</sup>, M. Juchno<sup>4</sup>, S. Krave<sup>1</sup>, M. Marchevsky<sup>3</sup>, J. Muratore<sup>2</sup>, F. Nobrega<sup>1</sup>, H. Pan<sup>3</sup>,  
J.C. Perez<sup>4</sup>, I. Pong<sup>3</sup>, S. Prestemon<sup>3</sup>, E. Ravaoli<sup>3</sup>, G.L. Sabbi<sup>3</sup>, C. Santini<sup>1</sup>, J. Schmalzle<sup>2</sup>, S. Stoynev<sup>1</sup>,  
T. Strauss<sup>1</sup>, G. Vallone<sup>4</sup>, P. Wanderer<sup>2</sup>, X. Wang<sup>3</sup>, M. Yu<sup>1</sup>

<sup>1</sup>Fermi National Accelerator Laboratory, Batavia IL 60510, USA

<sup>2</sup>Brookhaven National Laboratory, Upton NY 11973, USA

<sup>3</sup>Lawrence Berkeley National Laboratory, Berkeley CA 94720, USA

<sup>4</sup>CERN, CH-1211 Geneva 23, CH

### *Abstract:*

*This report presents the fabrication and QC data of MQXFS1, the first short model of the low-beta quadrupoles (MQXF) for the LHC High Luminosity Upgrade. It describes the conductor, the coils, and the structure that make the MQXFS1 magnet. Qualification tests and non-conformities are also presented and discussed.*

*The fabrication of MQXFS1 was started before the finalization of conductor and coil design for MQXF magnets. Two strand design were used (RRP 108/127 and RRP 132/169). Cable and coil cross-sections were “first generation”.*

**TABLE OF CONTENTS**

<b>1. CONDUCTOR CHARACTERISTICS</b>	<b>3</b>
<b>Strand</b>	
<b>Cable</b>	
<b>Insulation</b>	
<b>Estimate of magnet short sample limit</b>	
<b>2. COIL FABRICATION AND INSTRUMENTATION</b>	<b>11</b>
<b>Coil Fabrication</b>	
<b>Coil Instrumentation</b>	
<b>Electrical tests</b>	
<b>CMM results</b>	
<b>Non conformities</b>	
<b>3. STRUCTURE FABRICATION AND MAGNET ASSEMBLY</b>	<b>20</b>
<b>Shell-Yoke Subassembly</b>	
<b>Yokes</b>	
<b>Coil Pack</b>	
<b>Integration</b>	
<b>Instrumentation, Checkout and Magnet QC</b>	
<b>4. QUENCH PROTECTION</b>	<b>37</b>
<b>Quench Heater strips</b>	
<b>CLIQ terminals and leads</b>	

## 1. CONDUCTOR CHARACTERISTICS

### a. Strand

The two LARP coils in MQXFS1, QXFS03 and QXFS05 used cables P33OL1053A and P33OL1057B. They are both fabricated using OST RRP® 108/127 strands. These strands are Ti-doped and have Nb/Sn ratio of 3.6 (“reduced-Sn” type).

The strands were from the following billets: 14983, 14984, 14752, 14896 and 15519. These billets were initially qualified at 0.778 mm by OST. Subsequently, these billets which were held at 1.0 mm diameter were drawn down to 0.85 mm. Table 1.1, is a summary of the qualification data for which the strands were reacted at the high temperature plateau of 650 C/50h.

Table 1.1: Strand Parameters

Wire ID	Wire Dia.	lc(12T)	n(12T)	lc(15T)	n(15T)	Jc(12T)	Jc(15T)	NC%	RRR
	mm	A		A		A/mm <sup>2</sup>	A/mm <sup>3</sup>		
RRP-14752-BE	0.778	619	41	326	42	2914	1535	0.447	242
RRP-14752-FE	0.778	622	72	331	53	2864	1524	0.457	168
RRP-14896-BE	0.778	632	63	326	49	2898	1495	0.459	289
RRP-14896-FE	0.778	644	47	338	39	2902	1523	0.467	192
RRP-14983-BE	0.778	620	52	324	41	2849	1489	0.458	192
RRP-14983-FE	0.778	607	49	320	37	2771	1461	0.461	166
RRP-14984-BE	0.778	622	58	323	51	2815	1462	0.465	283
RRP-14984-FE	0.778	643	32	340	42	2904	1536	0.466	227
RRP-15519-BE	0.851	720	46	392	47	2690	1464	0.472	291
RRP-15519-FE	0.851	728	60	396	43	2702	1470	0.475	275

The strands after being drawn to 0.85 mm were found to be slightly larger than 0.853 mm which was set as the upper limit of wire diameter. Note that the wires used in the cable were pre-annealed at 170 C for 18 h.

Since the coils were reacted using a high temperature plateau of 640 C, some of the billets were checked with this lower temperature of reaction. At the lower temperatures the loss in Jc is very small as compared to that at the higher temperature of reaction. However, the RRR is increased by a large fraction. Table 1.2 summarizes the data for the strands tested.

Table 1.2: Tested Strands Parameters

Wire ID	Wire Dia.	lc(15T)	lc(12T)	Jc(15T)	Jc(12T)	NC%	RRR
RRP-14752-FE	0.850	379	727	1461	2805	0.457	334.2
RRP-14983-FE	0.850	382	728	1460	2737	0.461	369.7

The two CERN coils in MQXFS01, coil 103 and 104 used cable H16OC0164A and H16OC0164B. They are both fabricated using OST RRP® 132/169 strands. The strands properties are given in table 1.3 and 1.4.

Table 1.3: Wire Characteristics coil 103

Strand Type	<b>RRP 132/169</b>
Billets	<b>15948,15960,15962,16277</b>
non-Cu fraction	<b>46%</b>
Max $I_c(4.22\text{ K}, 12\text{ T})^{**}$	<b>Larger 745 A</b>
Min $I_c(4.22\text{ K}, 12\text{ T})^{**}$	<b>Lower 693 A</b>
Max RRR <sup>**</sup>	<b>221</b>
Min RRR <sup>**</sup>	<b>172</b>

\*\* Values (from OST) for virgin wires reacted for 48 hrs at 210 °C, 48 hrs at 400 °C, 50 hrs at 640 °C

Table 1.4: Wire Characteristics coil 104

Strand Type	<b>RRP 132/169</b>
Billets	<b>15948,15960,15962,16277</b>
non-Cu fraction	<b>46%</b>
Max $I_c(4.22\text{ K}, 12\text{ T})^{**}$	<b>Larger 745 A</b>
Min $I_c(4.22\text{ K}, 12\text{ T})^{**}$	<b>Lower 693 A</b>
Max RRR <sup>**</sup>	<b>221</b>
Min RRR <sup>**</sup>	<b>172</b>

\*\* Values (from OST) for virgin wires reacted for 48 hrs at 210 °C, 48 hrs at 400 °C, 50 hrs at 640 °C

The coil heat treatment was carried out on the GERO2500 furnace in building 927. The heat treatment schedule was the following: 48 hrs at 210 °C, 48 hrs at 400 °C, 50 hrs at 640 °C.

For coil 103, Five  $I_c$  witness samples were reacted with the coil and measured in building 163. Two samples were round wires and the other three were strands extracted from the same cable that was used to wind the coil. For coil 104, Six  $I_c$  witness samples were reacted with the coil and measured in building 163. Three samples were round wires and the other three were strands extracted from the same cable that was used to wind the coil. From these critical current measurements we can derive the parameters  $B_{c2}(4.3\text{ K})$ ,  $C(4.3\text{ K})$ ,  $B_{c2}(1.9\text{ K})$ ,  $C(1.9\text{ K})$  that allow describing the critical surface with the well-established function:

$$I_c \cdot B_{peak} = C(T)b^{0.5}(1 - b)^2 \quad \text{eq. 1.1}$$

where:

$$b \equiv B_{peak} / B_{c2}(T) \quad \text{eq. 1.2}$$

By using this formula to fit the critical current measurements of the witness samples, we obtain the parameters reported in Table 1.5 and 1.6. These parameters describe the critical current of the extracted witness sample with the lowest performance. The critical current of the extracted witness sample with the best performance can be estimated by multiplying the  $C$  parameter by 1.035 for coil 103 and 1.039 for coil 104.

Table 1.5:  $I_c$  Parameters coil 103

Temperature K	$B_{c2}$ [T]	$C$ [kA/T]
4.30	23.6	45.79
1.90	26.3	52.87

Table 1.6:  $I_c$  Parameters coil 104

Temperature K	$B_{c2}$ [T]	$C$ [kA/T]
4.32	23.53	47.97
1.90	26.3	55.47

The expected critical current of the cable is summarized in Fig. X and XX. In particular, the two thick lines show the critical current of the cable calculated by using the parameters in Table 1.5 and 1.6 for the strand critical current; those lines represent the minimum currents that we could expect from the witness samples at 4.30 and 1.90 K. In the same figure, the two thin lines show the expected maximum currents; these values are obtained via the parameters in Table IV after having multiplied  $C$  by 1.035 and 1.039.

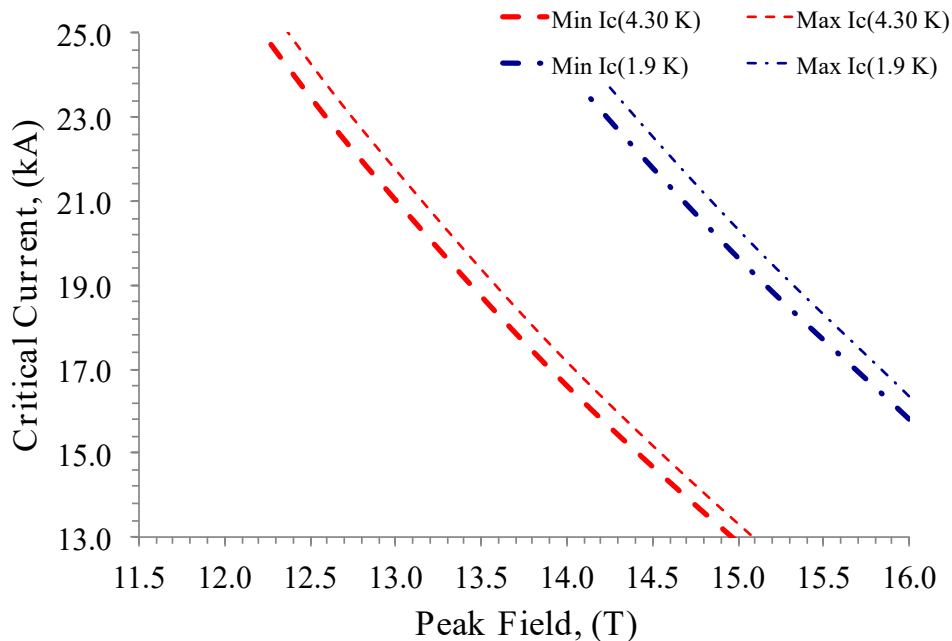


Fig. 1.1: Critical Surface for Coil 103.

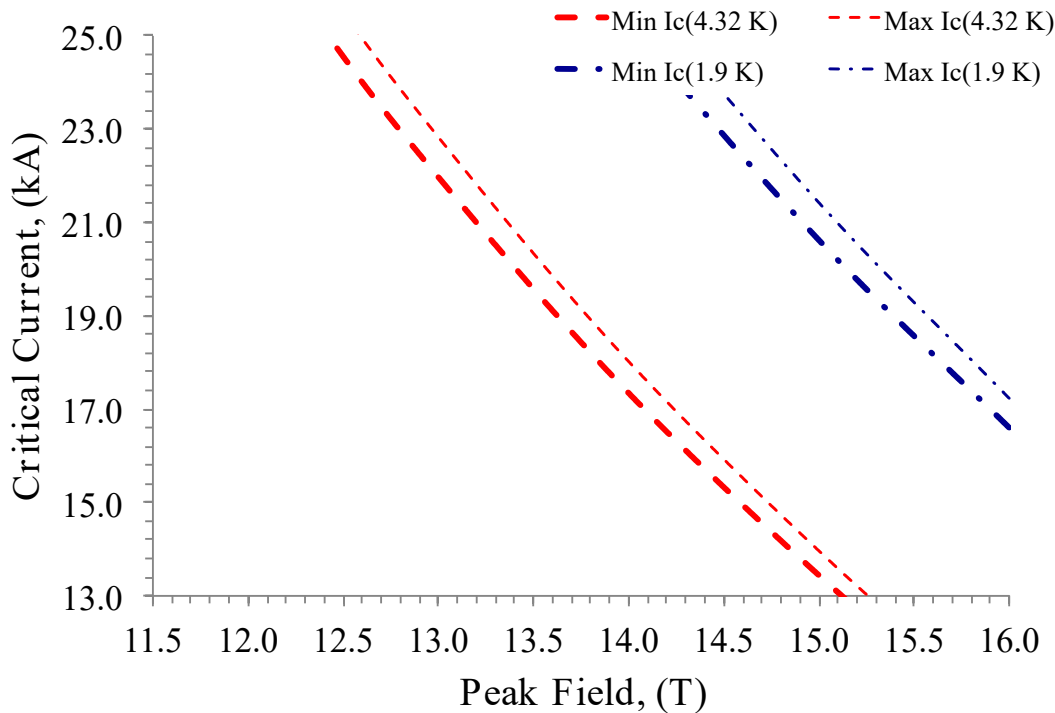


Fig. 1.2: Critical Surface for Coil 104.

Furthermore for coil 103, five RRR witness samples were reacted with the coil and measured in building 163: two virgin wires, which had a RRR equal to 212, 224, and; three extracted strands. The extracted samples had a RRR equal to 164, 178 and 186. For coil 104, six RRR witness samples were reacted with the coil and measured in building 163: three virgin wires, which had a RRR equal to 195-222, and; three extracted strands. The extracted samples had a RRR equal to 146, 157 and 172.

## b. Cable

The two LARP coils used in MQXFS1, QXFS03 and QXFS05, used cables P33OL1053A and P33OL1057B (see description below). They are both ‘first generation’ cables with a stainless steel core using 40 OST RRP® 108/127 strands. These strands are Ti-doped and have Nb/Sn ratio of 3.6 (“reduced-Sn” type). The strands were annealed at 170°C for 18 h before cable fabrication.

Cable P33OL1053A1 was fabricated in April 2014. 177 m of cable was made from 195 m of re-spooled strands. 3 m of archive sample was recorded. 174 m of cable was sent to NEWT for insulation.

Cable P33OL1057A was fabricated in August 2014 as a single piece 358 m long from 380 m of re-spooled strands. 18 m of archive sample (P33OL1057AD40A) was kept at LBNL, 3 m of which was sent to BNL for extracted strand measurements. 340 m of cable was sent to NEWT for insulation. While

the cable was at NEWT, LARP decided to section the cable into two pieces. NEWT was asked to cut the cable in equal lengths. However, NEWT cut the two into unequal lengths of 140 m and 200 m. It was identified that the longer piece came from the cable fabrication tail end, and the production unit identifier ‘B’ was retrospectively applied. P33OL1057B was used in coil QXFS05, with a 67.8 m drop after coil winding. For completion, the shorter cable piece P33OL1057A was used in coil QXFS04, with a 6.1 m drop.

The cable map details are summarized in Table 1.4.

Table 1.4: Cable Maps

Coil	Cable Map	Wire ID	No. of Re-spools
QXFS03	P33OL1053 Re-spooled length = 195 m Manufactured in April 2014	PO08S14752R01U	4
		PO08S14896N01U	34
		PO08S14984Q01U	2
QXFS05	P33OL1057 Re-spooled length = 380 m Manufactured in August 2014	PO08S14752C01A	2
		PO08S14752D01A	4
		PO08S14752F01A	10
		PO08S14983A01A	15
		PO08S14983B01A	4
		PO08S15519A01A	2
		PO08S15519C01A	3
Coil 103	H16OC0164A	HO08S15948A05U	2
		HO08S15960A03U	7
		HO08S15962A03U	5
		HO08S15948A02U	8
		HO08S15962A01U	3
		HO08S16277A03U	4
		HO08S16277A01U	11
Coil 104	H16OC0164B	HO08S15948A05U	2
		HO08S15960A03U	7
		HO08S15962A03U	5
		HO08S15948A02U	8
		HO08S15962A01U	3
		HO08S16277A03U	4
		HO08S16277A01U	11

Same salient production details and cable parameters are summarized in Table 1.5.

-----  
<sup>1</sup> At the time this cable was made, the ID Scheme was still being finalized. Two start-up lengths were made as 1053-A and 1053-B. The production unit was recorded as 1053-C, and persisted in some LBNL record as P33OL1053C. However, for all LARP purposes and in this report, the 174 m of production unit should be identified as P33OL1053A. From cable map number 1057 (P33OL1057) onwards, start-up lengths are identified by a number (e.g. P33OL1057<sub>1</sub>) and production units by letters (e.g. P33OL1057<sub>A</sub>).

Table 1.5: Cable Parameters

	QXFS03 P33OL1053A	QXFS04/05 P33OL1057A/B	Coil 103 H16OC0164A	Coil 104 H16OC0164B
Cable Twist	109 mm (Left Hand Lay)			
Top Roll ID	P87 (20130409)	P87 (20130409)	Po 27/01	Po 27/01
Bottom Roll ID	P88 (20130409)	P88 (20130409)	Pu 27/01	Pu 27/01
Roll Width	18 mm	18 mm	18.1 mm	18.1 mm
Roll Angle	0.6°	0.6°	0.56°	0.56°
Mandrel ID	27i7653 (20140421)	27i7683 (20140703)	LHCDCBTA144B	LHCDCBTA156A
Mandrel Width	17 mm	17 mm	16.7 mm	16.7 mm
Mandrel Thickness	0.6 mm	0.6 mm	0.5 mm	0.5 mm
Stainless Steel ID	100L01A0513646	119L01A0517863	1.4404	1.4404
Stainless Steel Core Dimension	10.(1) mm x 0.025 mm	11.9 mm x 0.025 mm	14 mm x 0.025 mm	12 mm x 0.025 mm
Stainless Steel Core Heat #	833643	842189	519361	523435
Stainless Steel Core Lot #	11-501	14-363	519361	523435
Length Produced	177 m	358 m	156m	160m
Averaged Mid-Thickness <sup>1</sup>	1.523 mm ( $\sigma = 0.002$ mm)	1.522 mm ( $\sigma = 0.001$ mm)	1.526 mm ( $\sigma = 0.004$ mm)	1.5227 mm ( $\sigma = 0.002$ mm)
Averaged Width <sup>1</sup>	18.146 mm ( $\sigma = 0.002$ mm)	18.125 mm ( $\sigma = 0.002$ mm)	18.140 mm ( $\sigma = 0.003$ mm)	18.140 mm ( $\sigma = 0.002$ mm)
Averaged Keystone Angle <sup>1</sup>	0.540° ( $\sigma = 0.014^\circ$ )	0.581° ( $\sigma = 0.012^\circ$ )	0.562° ( $\sigma = 0.020^\circ$ )	0.576° ( $\sigma = 0.024^\circ$ )

Cable parameters were measured by LBNL-CME#1 during fabrication at nominal pressure of 17 MPa.

**c. Insulation**

The results of the insulation thickness measurements and the cable length before and after insulation are presented in Table 1.6.

Table 1.6: Insulation Parameters

	QXFS03 P33OL1053A	QXFS05 P33OL1057B	Coil 103 H16OC0164A	Coil 104 H16OC0164B
Insulation Thickness (vendor)	0.147 mm	0.145 mm	N/A	N/A
Insulation Thickness (verification)	0.144 mm	0.139 mm	0.147 mm	0.142-0.145 mm
Length sent to vendor	174 m	340 m	156 m	160 m
Length received by FNAL	169	195	156 m	160 m

**d. Estimate of magnet short sample limit**

Fig. 1.3 shows the magnet load-line and the critical surfaces for each coil.

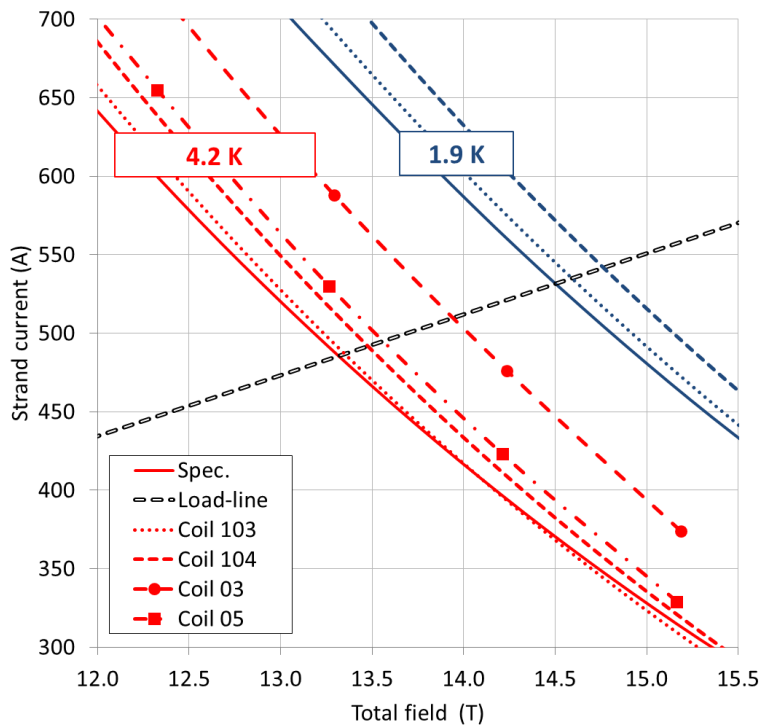


Fig. 1.3: Strand critical currents vs. total magnetic field (including self-field correction): values from strand specifications, and fit curve of measurements performed on extracted strand data from coils 103 and 104.

According to extracted strand measurements, the expected maximum current for each coil and for the MQXFS1 magnet is provide in Table 1.7.

Table 1.7: Expected maximum current

Short-sample						
	Current	Field	Gradient	Current	Field	Gradient
	4.3 K	4.3 K	4.3 K	1.9 K	1.9 K	1.9 K
	kA	T	T/m	kA	T	T/m
Coil 103	19.550	13.383	155.164	21.50	14.599	169.083
Coil 104	19.775	13.525	156.783	21.78	14.769	171.026
Coil 3	20.118	13.740	159.245	22.28	15.080	174.573
Coil 5	19.725	13.493	156.424	21.85	14.813	171.526
Magnet	19.550	13.383	155.164	21.50	14.599	169.083

## 2. COIL FABRICATION AND INSTRUMENTATION

MQXFS01 is comprised of 2 coils fabricated by LARP and 2 coils fabricated by CERN. All coils are of the first generation variety with identical designs converged upon by both BEND and ROXIE software packages. In this section we will not repeat the fabrication techniques presented in the QXF first generation design report [1]. Here we highlight the key fabrication parameters and measurements that uniquely distinguish each coil.

Table 2.1: Coil Overview

COIL #	W&C Location	R&I Location	GENERAL FABRICATION COMMENTS
Coil 3	FNAL	BNL	Coil oversize by 40 $\mu\text{m}$ at each midplane. Passed all electrical tests. (108/127 strand)
Coil 5	FNAL	BNL	Passed all electrical tests. (108/127 strand)
Coil 103	CERN	CERN	Keyway shifted toward transition side by 60 $\mu\text{m}$ near return end. Passed all electrical tests. (132/169 strand)
Coil 104	CERN	CERN	Undersize by 85 $\mu\text{m}$ at each midplane. Passed all electrical tests. (132/169 strand)

### a. Coil Fabrication

The pole pieces for each coil were procured by LARP and the end parts were procured by rapid prototyping by CERN. This provides a high level of tooling consistency for all coils in MQXFS1. The insulation materials and thicknesses are slightly different between CERN and LARP for 1<sup>st</sup> generation coils. Measured insulation thicknesses for MQXFS1 coils are highlighted in Table 2.2.

Table 2.2: Insulation Thicknesses

Thickness @ 5 MPa ( $\mu\text{m}$ )	Nominal	Coils 3 and 5		Coils 103 and 104	
		W & C	R & I	W & C	R & I
Cable Insulation	150	139 - 145	N/A	142-147	N/A
ID/OD Reaction	250	Not Used	174 (2 layers, Plain fabric)	Not Used	173 (2 layers, Plain fabric)
ID/OD Impregnation	150	Not Used	121 (1 layer)	Not Used	not measured
Interlayer (w/ binder)	500	518	490	476	482
Tape in the ends (w/ binder)	175	230 (ends)	213	174	166
Tape around pole (w/o binder)	175	174	N/A	119	N/A

The amount of binder is significantly different between coils. For the above table the thickness measurements were performed with amounts of binder identical to that used on actual coils. As a general rule LARP applied more binder than CERN. The nominal amounts of binder for short coils is summarized in the below table. To prevent popped strands near the ends LARP uses binder and CERN uses the winding tool that prevents popped strands.

The entire coil is cured with binder after winding. This suggests that the usable thickness of each fabric should be measured with binder applied in an amount and pressure identical to the curing process. This is difficult since the coil pressures vary significantly. A standard measurement pressure of 5 MPa was chosen for measurement comparisons.

Binder does not directly cause insulation to expand. Binder adds rigidity to insulation and artificially increases thickness if allowed to cure without compression. In other words, the fabric thickness is determined by the cavity or thickness with which the fabric was cured in. The added thickness remains through heat treatment and subsequent impregnation.

Table 2.3: Binder Amounts

	<b>Coils 3 and 5</b>	<b>Coils 103 and 104</b>
Ends of each turn	Minimal amount	Not Used
Interlayer Insulation	31 grams / meter	49 grams / meter
Layer 1 Curing	90 grams	59 grams (33 g on middle + 13 g on each side)
Layer 2 Curing	120 grams	59 grams (33 g on middle + 13 g on each side)

The braided on cable insulation for both CERN and LARP have identical specifications but slightly different braid parameters. Braided on cable insulation constricts growth during heat treatment and the expansion is substantially less than allowed for by design. CERN insulation is braided on with 32 carriers while LARP insulation is braided on with 48 carriers. To maintain similar insulation thickness, CERN insulation preferentially constricts cable width growth. LARP insulation allows more coil shrinkage/pole gap closure. All coils fabricated to date, including MQXFS1 coils, follow this trend. Dimensional change during fabrication are summarized below for MQXFS coils. Cable property data is based on practice coil cross sections.

Table 2.4: Fabrication Dimensional Changes

Property (Nominal)	Cable Properties		L2 Pole Gap Closure (mm)				
	Thickness (4.5%)	Width (2.5%)	Initial Gap	$\Delta$	Before Reaction	$\Delta$	After Reaction
<b>Coil 3</b>	~3.2%	~0.3%	3.89	2.04	1.85	<b>1.39</b>	0.46
<b>Coil 5</b>	~3.2%	~0.3%	3.65	1.64	2.01	<b>1.65</b>	0.36
<b>Coil 103</b>	~3.2%	~0.1%	4.5	1.39	3.11	<b>0.47</b>	2.64
<b>Coil 104</b>	~3.2%	~0.1%	2.0	1.6	0.4	<b>-0.1</b>	0.5

Table 2.5: Heat Treatment Properties

Coil	Inlet Gas Flow (SCFH)		HT Profile					
	Oven/Retort	Tooling	Temp 1	Soak 1	Temp 2	Soak 2	Temp 3	Soak 3
<b>Coil 3</b>	50	25	210°C	72 h	400°C	48 h	637°C	48 h
<b>Coil 5</b>	50	25	211°C	72 h	401°C	48 h	641°C	48 h
<b>Coil 103</b>	71	12	210°C	47 h	400°C	51 h	639°C	52 h
<b>Coil 104</b>	71	12	209°C	53 h	400°C	49 h	640°C	50 h

**b. Coil Instrumentation**

All MQXFS coils were instrumented with voltage taps, protection heaters, and strain gauges. The following table and subsequent charts describe the instrumentation installed specific to each coil. Also included are the known instrumentation issues. All lost heaters and gauges occurred during cool down and initial cold checkouts.

Table 2.6: Voltage Taps, Protection Heaters, & Strain Gauges

Coil	Voltage Taps	Protection Heaters		Strain Gauges	
		Design	Lost Heaters	Design	Lost Gauges
<b>Coil 3</b>	None Lost	LARP – SS only OL, SS/Cu IL		Axi + Azi for DC LARP Style and Axi + Azi for AC CERN Style	Lost LARP Azi
<b>Coil 5</b>	None Lost	LARP – SS only OL, SS/Cu IL	A01 failed cold ~700 V	Axi + Azi for DC LARP Style and Axi + Azi for AC CERN Style	
<b>Coil 103</b>	None Lost	CERN – Cu/SS design	A02 failed cold ~700 V	Axi + Azi for DC LARP Style and Axi + Azi for AC CERN Style	Lost LARP Axi
<b>Coil 104</b>	A03 was installed on turn 11 instead of Turn 6, None Lost	CERN – Cu/SS design	A02 failed cold ~700 V	Axi + Azi for DC LARP Style and Axi + Azi for AC CERN Style	Lost LARP Azi

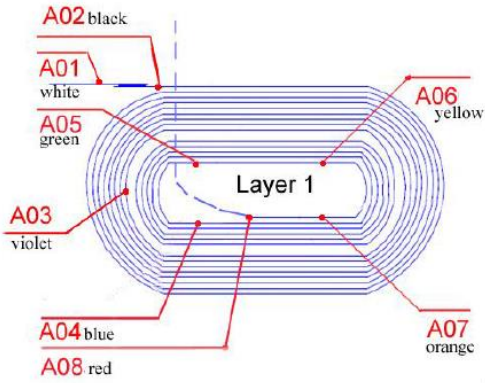


Fig. 2.1: Coil Voltage Tap Map Layer 1.

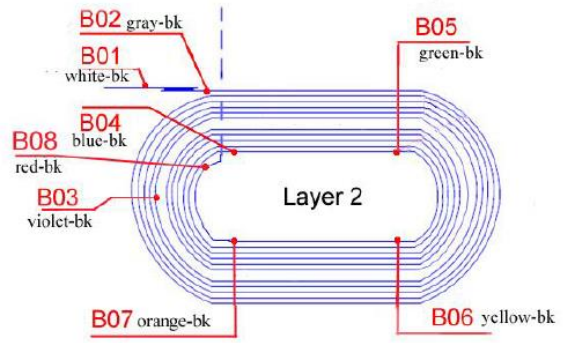


Fig. 2.2: Coil Voltage Tap Map Layer 2.

MQXFS1 Magnet Schematic

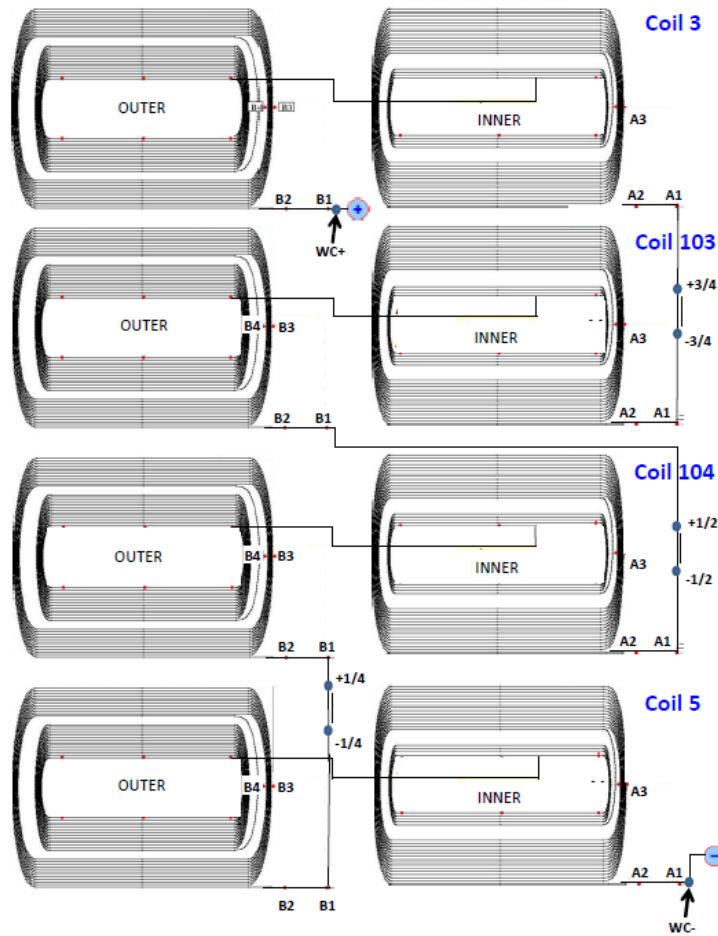


Fig. 2.3: Magnet Voltage Tap Map

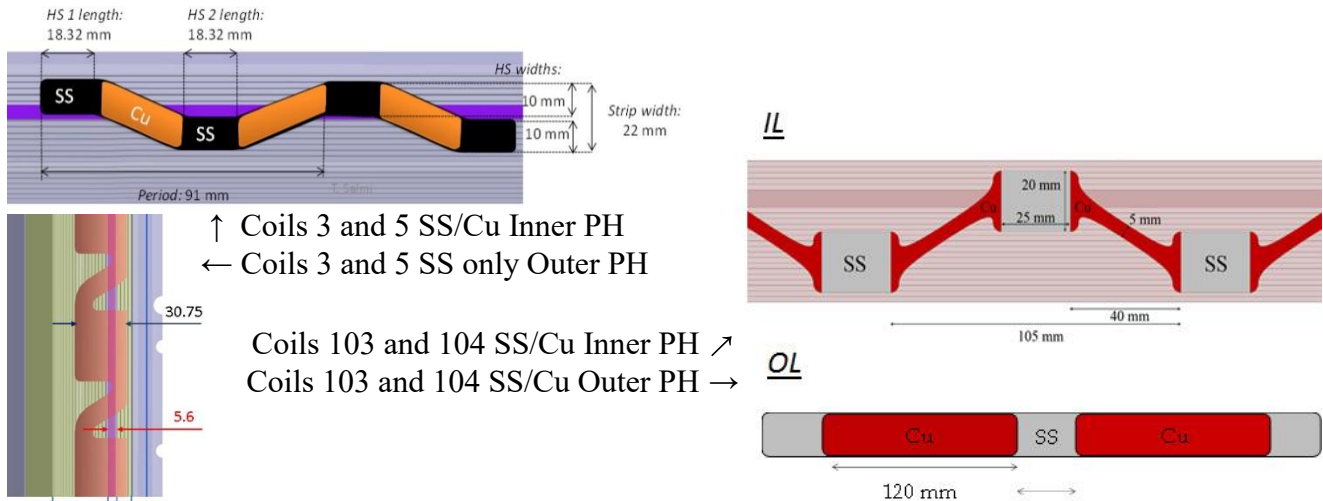


Fig. 2.4: Protection Heater Designs

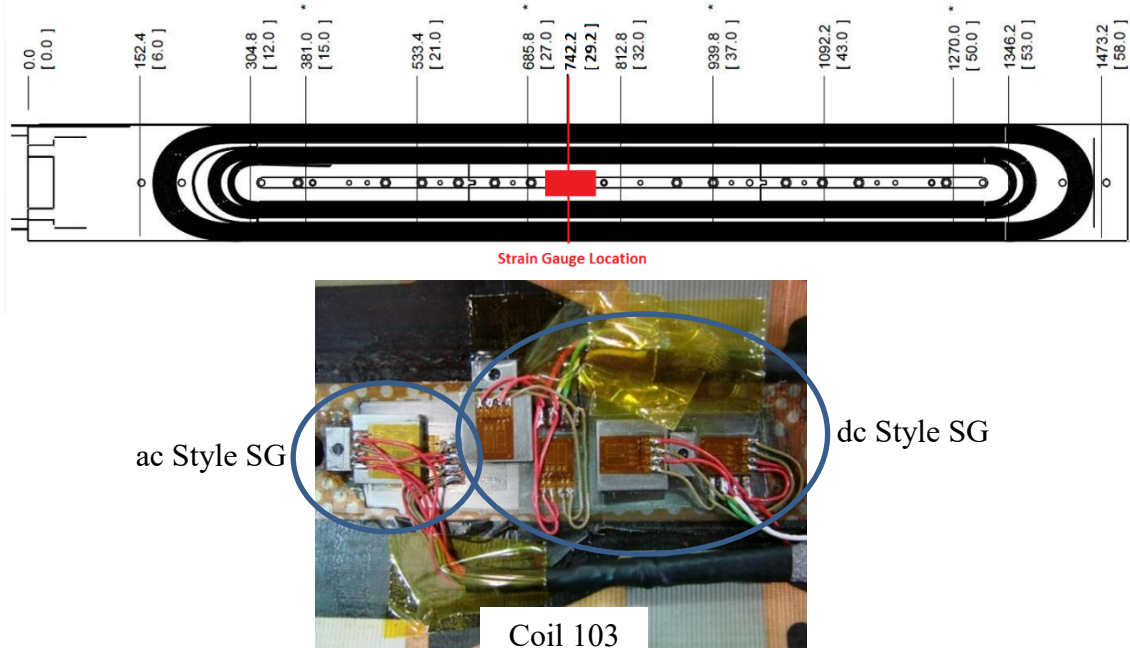


Fig. 2.5: Coil Strain Gauge Location and CMM Locations

### c. Electrical tests

All coils passed nominal electrical hi-pot and impulse tests. For reference the hi-pot and impulse test data for coil 5 is provided below. The only difference is that coils 103 and 104 impulse tests were to 2.5 kV and coil 3 and 5 tests were to 2.0 kV. An electrical measurement summary after coil impregnation is also presented below. All tests were at room temperature.

SQXF05		Coil		Hipot Checks							
PHA01	2500 / 2500			Actual / Target							
PHA02	2500 / 2500	PHA01	PHA02	(< 1 uA leakage)							
PHB01	2500 / 2500										
PHB02	2500 / 2500			PHB01	PHB02	PHB03	PHB04				
PHB03	2500 / 2500										
PHB04	2500 / 2500										
LE IL Endshoe	1000 / 1000	2500 / 2500	2500 / 2500						LE IL Endshoe	RE IL Endshoe	
LE OL Endshoe	1000 / 1000			2500 / 2500	2500 / 2500	2500 / 2500	2500 / 2500	2500 / 2500	600 / 600		
RE IL Endshoe	1000 / 1000	2500 / 2500	2500 / 2500								
RE OL Endshoe	1000 / 1000			2500 / 2500	2500 / 2500	2500 / 2500	2500 / 2500	2500 / 2500		600 / 600	
Pole	500 / 500										

Fig. 2.6: QXFS05 HiPot Data

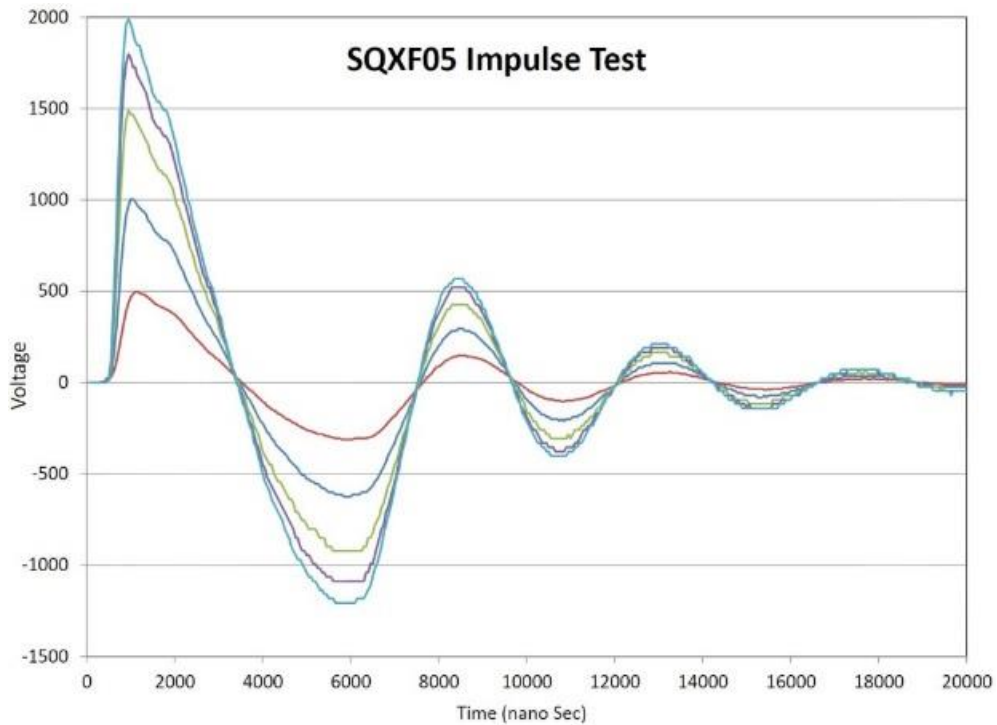


Fig. 2.7: QXFS05 Impulse Test Plots

Table 2.7: MQXFS Coils Electric Data

Post Impreg Data		Coil 3		Coil 5		Coil 103		Coil 104	
Coil R @ 1A (mV)		179.02		181.97		185.17		185.33	
L <sub>s</sub> @ 20 Hz (mH)	Q value	1.913	1.25	1.915	1.23	N/A	N/A	N/A	N/A
L <sub>s</sub> @ 100 Hz (mH)	Q value	1.733	3.41	1.767	3.32	1.772	N/A	1.767	N/A
L <sub>s</sub> @ 1 kHz (mH)	Q value	1.066	2.00	1.110	2.04	1.623	N/A	1.610	N/A
Voltage Taps (mV)	A1 (Inner)	0.174		0.015		0		0	
@ 1 A for Coils 3 and 5	A2	0.224		0.065		0.17		0.22	
@ 6 A for 103 and 104	A3	59.26		60.15		61.29		43.47	
Coil 103 & 104 (÷ 6)	A4	75.53		76.685		78.06		78.03	
	A5	75.76		76.917		78.30		78.27	
	A6	77.14		78.323		79.72		79.68	
	A7	77.35		78.534		79.92		79.90	
	A8	78.33		79.529		80.95		80.92	
	B8	78.73		79.956		81.37		81.35	
	B7	78.95		80.169		81.58		81.57	
	B6	80.26		81.508		82.93		82.90	
	B5	80.51		81.758		83.18		83.17	
	B4	81.83		83.094		84.55		84.53	
	B3	121.67		123.56		125.72		125.75	
	B2	178.82		181.71		184.99		185.04	
	B1 (Outer)	178.87		181.75		185.15		185.31	
Quench Heater	A01 (L1,R)	1.37		1.379		0.9318		0.9748	
(Ω)	A02 (L1,L)	1.42		1.386		0.9285		0.9667	
	B01 (Low,L)	3.23		3.132		0.6481		0.6621	
	B02 (High,L)	3.21		3.123		0.5995		0.6157	
	B03 (High,R)	3.27		3.182		0.6076		0.6215	
	B04 (Low,R)	3.31		3.195		0.6551		0.6692	

## d. CMM Results

As a general rule CERN QXF short coils are smaller in size than LARP coils. Variation along the length is relatively small and should have provided for a uniform preload during magnet assembly. The three plots below are from CMM data collected at LBNL with a coil OD and Keyway best fit. Azimuthal Coil size is the total deviation from nominal of the left and right midplanes. Keyway shift is the amount that the keyway is shifted with respect the nominal position. The deviation from nominal OD is the amount that a best fit circle to the coil OD deviates from the nominal outer diameter.

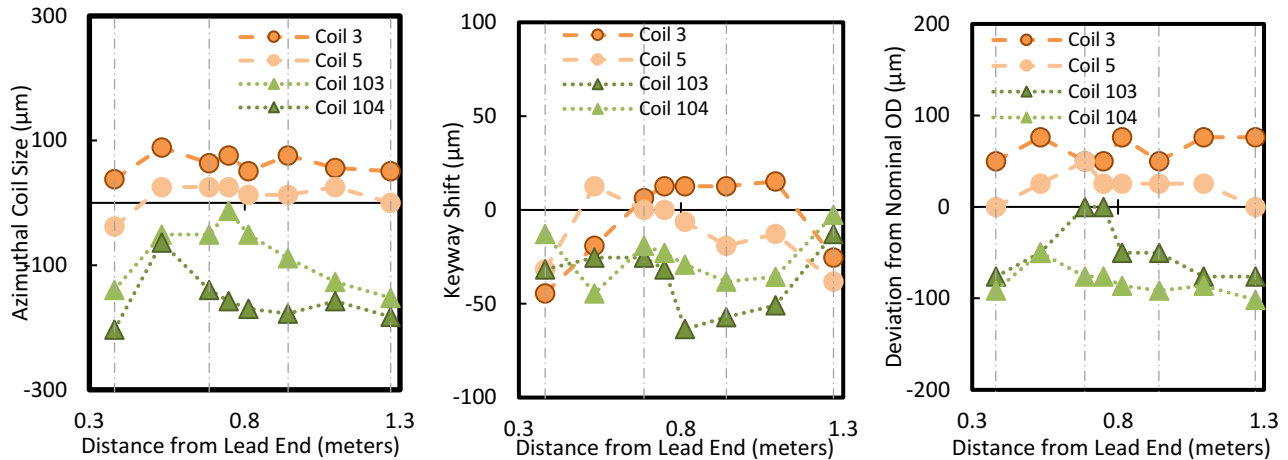


Fig. 2.8: CMM Results.

All coils seem to be the largest between 0.5 and 0.8 meters from the lead end coil edge. All coils seem to be the smallest near the coil ends. Coil ends are designed to be slightly undersized to prevent over compressing leads during fabrication and magnet assembly. MQXFS1 will be the first LARP quadrupole assembled with the bladder and key technique with coils of substantially different sizes. The size variation between coils necessitated specialized asymmetric shimming during magnet assembly and is described in detail in the magnet assembly section.

For each coil there seems to be a slight bias for the keyway to be shifted toward the left side of each coil. The magnitude of this asymmetry is quite small and well within expected values for MQXFS1 fabrication techniques and tooling.

The CERN coils have a slight concave shape as seen in the Deviation from Nominal OD plot while the LARP coils have a slight convex shape. These deviations were accommodated in part by the MQXFS1 assembly shim package.

## e. Non Conformities

All coil fabrication non conformities are minor and should pose no ill effects on magnet performance.

Table 2.8: Non Conformities

COIL #	W&C Non Conformities	R&I Non Conformities	Instr. Non Conformities
<b>Coil 3</b>	<ul style="list-style-type: none"> <li>• Reverse easy way bend on spool.</li> <li>• Minor bowing of pole piece.</li> <li>• Minor Insulation Fray</li> </ul> <a href="#">REPORTS</a> [2]	Temperature variation of 6°C at 640°C soak.	Lost LARP Azi SG
<b>Coil 5</b>	Wedge stains and transition insulation shift. <a href="#">REPORTS</a> [3]	B7 and A2 VTs need repair after impreg.	PH-A01 failed cold ~700 V
<b>Coil 103</b>	<ul style="list-style-type: none"> <li>• Interlayer slightly thinner than nominal (0.44 mm versus 0.5)</li> <li>• Pins between inner and outer pole slightly magnetic near ends.</li> </ul>	Some impregnation dry spots in coil MP and ID near the ends	PH-A02 failed cold ~700 V Lost LARP Axi SG
<b>Coil 104</b>	<ul style="list-style-type: none"> <li>• Loss of tension during winding of first turn of IL: tension recovered manually. VTAPS displaced of about 5 mm.</li> <li>• Pins between inner and outer pole pieces slightly magnetic near ends.</li> <li>• The VTAP A03 of the inner layer was installed on turn 11 instead of Turn 6.</li> </ul>	<ul style="list-style-type: none"> <li>• No pole gap closure during Heat treatment.</li> <li>• Accidental high flow argon purge caused ~5°C dip in temperature for 15 h during 210°C soak.</li> <li>• Vacuum test before impregnation: mold and coil in short cut, not possible to measure the capacitance.</li> </ul>	PH-A02 failed cold ~700 V Lost LARP Azi SG

## References

- [1] G. Ambrosio, P. Ferracin, et al., “MQXFS1 Design Report” (<http://larpdocs.fnal.gov//LARP-public/DocDB/ShowDocument?docid=1074>).
- [2] <https://vector-offsite.fnal.gov/Tools/DiscrepancyReport/DisplayDiscrepancyReportReadOnly.asp?qsDRNo=10386>
- [3] <https://vector-offsite.fnal.gov/Include/DisplayAllDRs.asp?qsDocID=16112>

### 3. STRUCTURE FABRICATION AND MAGNET ASSEMBLY

#### a. Shell-Yoke Subassembly

The shells were fabricated in Europe under a CERN procurement contract, were measured, and then shipped to LBNL for assembly. Each individual shell was then measured again in a Zeiss Accura CMM Inspection and post-processed in the Calypso software. The cylindricity was measured, and the average radii were also measured at 5 locations along the length of each shell. The two measurement sets (taken at CERN and LBNL) both matched, confirming the measured dimensions.

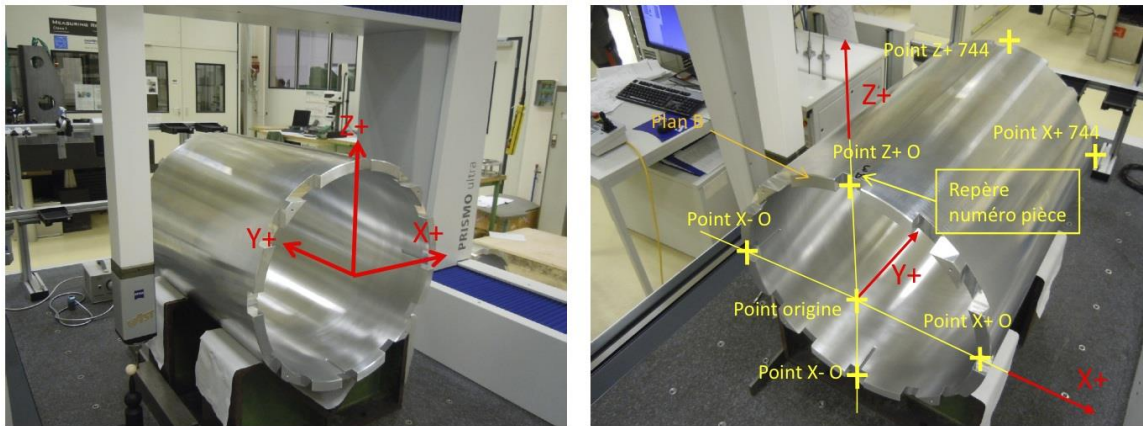


Fig. 3.1: (Left) A shell being measured at CERN. (Right) Axes conventions shown on the left; “Repere numéro pièce” refers to the identifying location mark on each shell.

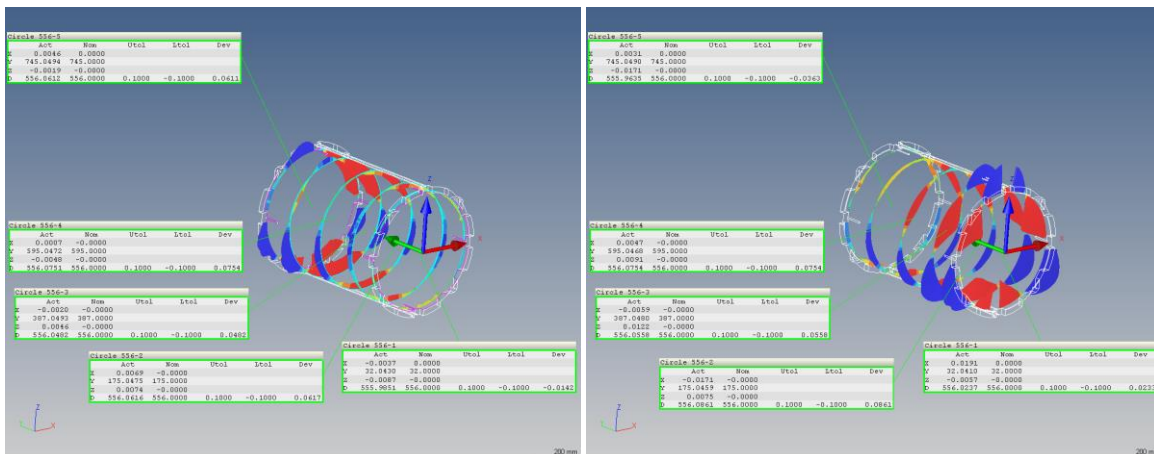


Fig. 3.2: (Left) Shell #1 measurements. (Right) Shell #4 measurements.

Table 3.1: Average diameters (calculated from the CMM measurement data), as a function of axial position.

Axial location	Shell 1 Avg. dia. (mm)	Shell 4 Avg. dia. (mm)
A: Pos. 32 mm	555.9851	556.0237
B: Pos. 175 mm	556.0616	556.0861
C: Pos. 387 mm	556.0482	556.0558
D: Pos. 595 mm	556.0751	556.0754
E: Pos. 745 mm	556.0612	555.9635

After the receipt of the shells from CERN, the decision to split one of the shells was made [1], which would minimize the stress variations along the length of the magnet due to the shell cutouts. Therefore, after a comparison of the shell measurements (Table 3.1) it was decided to split Shell 4 so that cut faces (position “C”) mated up with the ends of Shell 1 (Positions “A” and “E”); see Figure 3.3.

The maximum diameter of all measurements is 556.0861 mm (section 4B), and the minimum is 555.9635 mm (section 4E), for a maximum diameter variation of  $\sim 123 \mu\text{m}$  from end to end, or  $\sim 0.005\%$ . In this cut shell orientation section 4C matches up with sections 1A and 1E, and would cause a small step (on the order of  $\sim 35 \mu\text{m}$  radially) towards the LE of Shell 1; there's virtually no step towards the RE of Shell 1. Per the ANSYS model results, a shell radial deviation of  $\sim 50 \mu\text{m}$  represents roughly a 10% variation in coil preload stress.

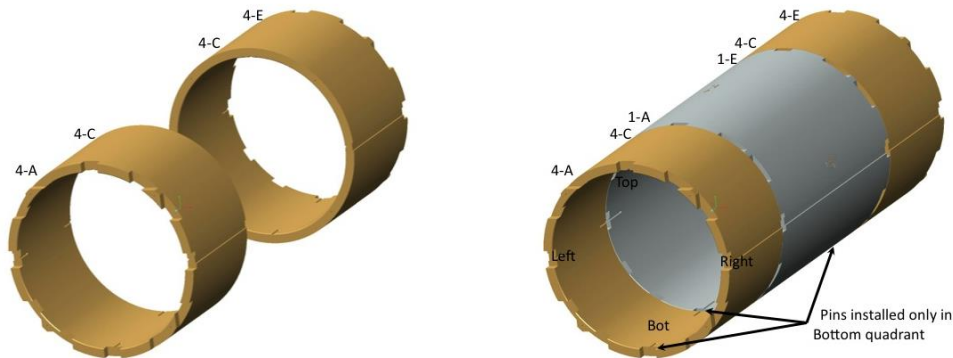


Fig. 3.3: Shell order and configuration (Left) Shell 4 cut sections, (Right) oriented with Shell 1. Both views from the LE.

Each half was machined to 385 mm long, which equates to a 770 mm combined length (or a total loss of 4 mm length from the 774 mm long shell). The original cutouts in these shell ends are all 25 mm deep prior to a refinement of the design where the final design of the MQXFA shells, which reduced these cuts to 15 mm deep for the yoke cutouts, while maintaining 25 mm deep for the welding block locations. In the case of the cut shell faces did not require any further cutouts, though pin slots were machined at the cut faces; however, not all the pin grooves lined up with those at the ends of Shell 1.

**b. Yokes**

The yokes were procured by CERN as full quadrant stacks that came machined and preassembled, and then delivered to LBNL. These assemblies were measured by CERN and confirmed by LBNL’s measurements as well, using the Zeiss Accura system. The yoke stacks each measured 1550 mm long. When assembled with the stacked shell segments, the yoke stacks are proud by 3 mm on each end when compared to the shells; prior to cutting the shell, they were designed to be only 1 mm proud on each end.

- **Yoke-shell subassembly**

Yoke stacks were inserted into the stacked shells in order and preloaded with a total of 12.14 mm (4.78”) of gap keys and shims; at this gap, the azimuthal shell gauges average was measured at 230 +/- 17  $\mu\epsilon$ . Nominal gap should be 12 mm, but an 11 mm gap key was shimmed with an additional 0.045” (or 1.14 mm) stack of shims in this step. [2]

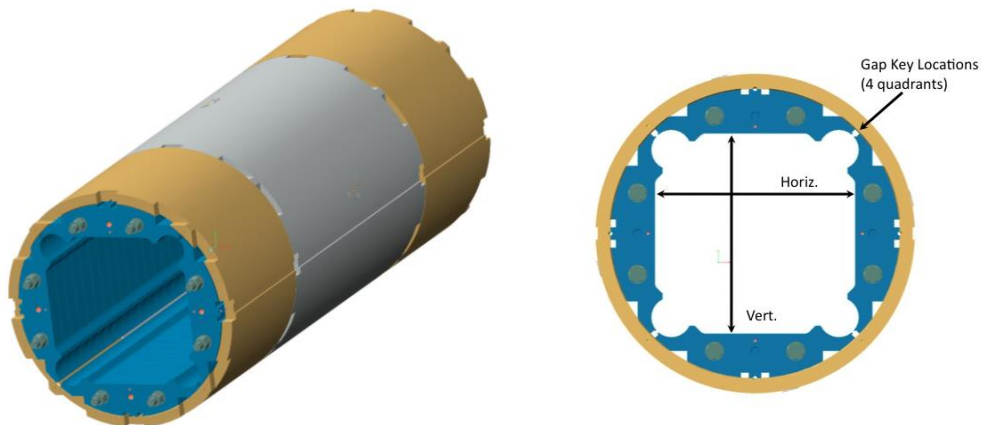


Fig. 3.4: (L) Shell-Yoke subassembly. (R) Gap keys and measurement locations.

Figure 3.4 shows the shell-yoke subassembly. The average final opening of the yoke-shell assembly with this gap key package was 15.173” / 385.39 mm in the vertical direction, and 15.171” / 385.34 mm, prior to the MQXFS-D mechanical model assembly. After the assembly, 77 K cool down test, and disassembly of that structure, the same gap key shim package was inserted (12.14 mm total). The dimensional size of the opening was measured to be 15.166” / 385.22 mm in both the vertical and horizontal directions. The average shell strain was still measuring at 230, however the spread was +/- 25  $\mu\epsilon$  before the assembly of MQXFS1. See Table 3.2.

Table 3.2: Shell measurements before and after the 77 K cool down test and disassembly.

	Gap key package, mm	Shell Strain Avg (T), $\mu\epsilon$	Vert opening, mm	Horiz. opening, mm
Initial subassembly, MQXFSD	12.14	230 +/- 17 $\mu\epsilon$	385.39	385.34
Post-77 K test and disassembly (prior to MQXFS1 Preload)	12.14	230 +/- 25 $\mu\epsilon$	385.22	385.22

### c. Coil Pack

- **Collar pack subassembly**

The Collar pack is a subassembly of the Coil pack, which is only the four coils surrounded by the collar lamination stacks; no load pads were assembled at this stage, aside from the bottom load pad stack; see Figure 3.5. Two of the coils were reacted and impregnated at BNL, and the other two were fabricated in CERN, and shipped to LBNL for assembly. See Section 2 for more details on the fabrication of the coils.

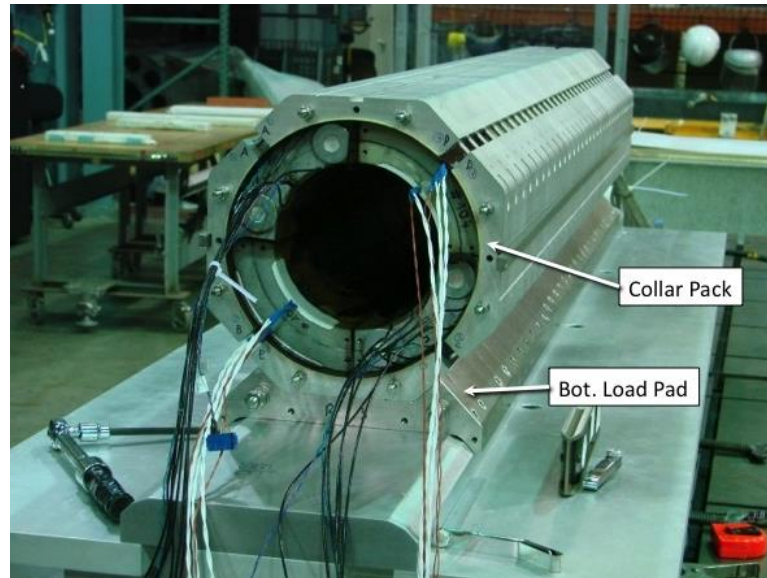


Fig. 3.5: Collar pack assembly.

CMM measurements were performed on all coils at the locations indicated in Figure 3.6. Measurements in the straight section showed that the CERN coils were smaller than the LARP-produced coils. See Table 3.3. Figure 3.7 shows side by side plots of the same axial location in each coil for comparison. All coils showed some left-right asymmetry, but we did not take this into account in any of the shimming packages.

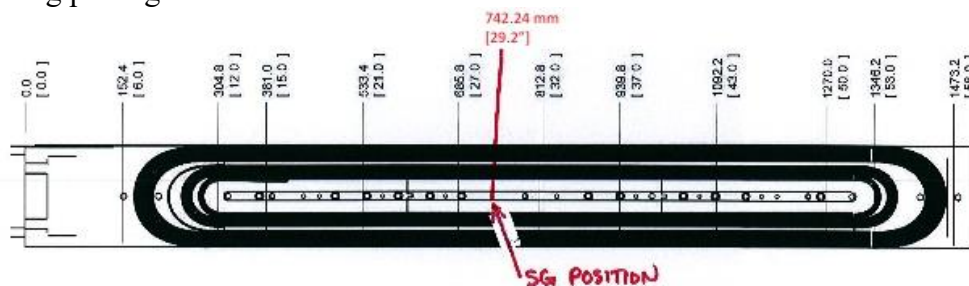


Fig. 3.6: Axial locations of the coil CMM measurements.

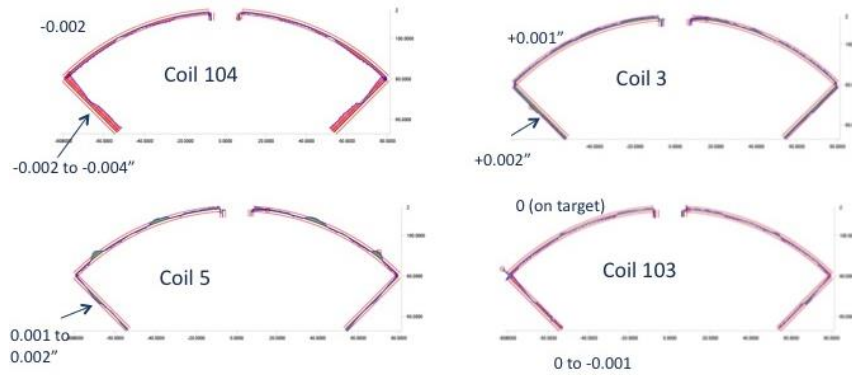


Fig. 3.7: CMM Measurements of all four coils of MQXFS1, at the same axial location.

Table 3.3: Coil size variances from nominal, determined by the CMM measurements.

	Azim. Size (Midplane), in	Radial Size, in	Azim. Size (Midplane), mm	Radial Size, mm
<b>LARP Coil 3</b>	+ .002	+ 0.001	+ 0.050	+ 0.025
<b>LARP Coil 5</b>	+ .002	~ 0	+ 0.050	~ 0
<b>CERN Coil 103</b>	~ 0	- 0.001	~ 0	- 0.025
<b>CERN Coil 104</b>	-0.003 to -0.004	- 0.002	-0.075 to -0.100	- 0.050

Because of the variations in the coil sizes, it was determined that the radial shimming be performed to align the effective mechanical OD of the coils in the same location; see Figure 3.8. See reference [3].

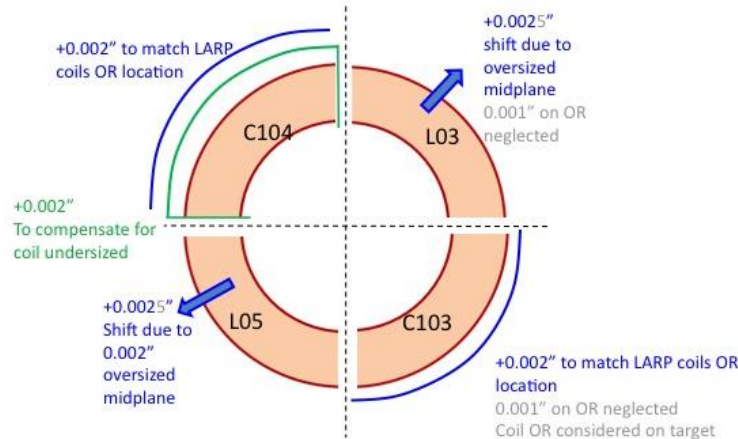


Fig. 3.8: Coil shimming plan, to deal with the different sizes of each coil; as viewed from the LE.

Coils then had Ground Plane Insulation (GPI) applied to the outer radius and the midplanes. This is a 0.005” thick Polyimide with B-stage epoxy, applied by a flat hobby iron. In determining the radial package of the collars, a nominal 0.0639” / 1.624 mm amount of shimming between the collars and the coils is required. Correcting for the actual measured coils, it was determined that there should be 0.0615” (~0.0025” less) shim package applied, theoretically. Therefore the initial radial shim package assembled was made of (0.005” coil GPI +) 0.007” (Fuji paper) + 5x 0.009” (G10) + 0.005” (G10), or 0.062” / 1.57 mm.

Assemblies using pressure sensitive (“Fuji”) paper are initially performed to verify good surface contact between the radial surfaces of the collars and coils. Super Low Pressure Fuji paper (70-350 psi / 0.5-2.0 MPa range) was used in the initial assemblies. At this stage, the Collar pack assembly builds often require several assembly/disassembly iterations to make radial shim package adjustments; in the case of MQXFS1 a total of four iterations were required before the fifth and final build was considered acceptable to proceed. During the disassembly of the second Collar pack assembly, an incident occurred where two coils experienced an uncontrolled fall to the assembly table. This incident is further described at the end of this section, and in more detail in [4].

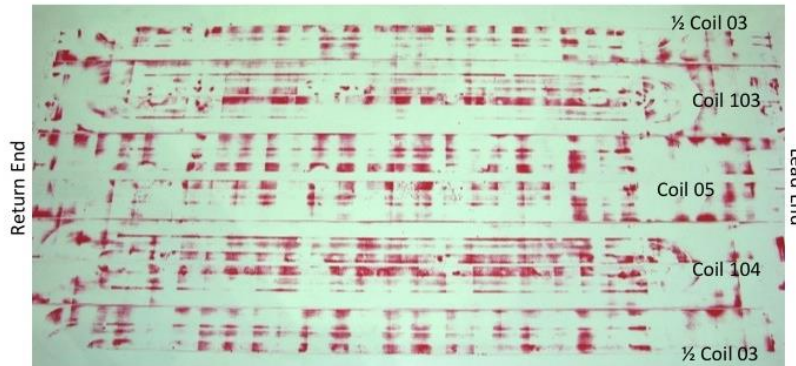


Fig. 3.9: Fuji paper exposure. From top to bottom: 1/2 Coil 03, Coil 103, Coil 05, C104, 1/2 Coil 03.

The first and third Collar pack builds were built using Fuji paper in the shim package, the difference being in the radial shim package reduction of 0.005” from the initial 0.062” stack, or 0.057” thick. The exposed Fuji paper of the third build showed an acceptable pattern of pressure in the coils; see Fig 3.9. The gaps between the collars are measured at this stage, and from this data the shim package of the coil alignment keys was calculated and prepared.

The fourth Collar pack build introduced the shimmed alignment keys installed in each coil, while also replacing the Fuji paper with the equivalent-thickness Kapton layers in the radial shim package. The measurements of collar-alignment key gaps showed that we needed another ~0.0015” (average) of shim per side on each alignment key, and so a new shim package was prepared for the keys and the Collar pack was disassembled and reassembled a last time with this change. The fifth and final Collar pack build showed no gaps at the collar/key interface, therefore we were assured of good contact in both the radial and alignment key surfaces. A summary of the final shim package is shown in Table 3.4.

Table 3.4: Final radial shim package of the MQXFS1 Collar Pack (5).

From Coil OR to Collar	L03	C103	L05	C104
Ground Plane Insulation (GPI)	0.005” (0.125 mm)			
Coil Specific Shim	0	0.002” (0.050 mm)	0	0.004” (0.100 mm)
Fuji Paper	N/A			
G10 + Kapton Radial Shim	5x0.009” + 0.002” + 0.005”			
Alignment Key thickness	14.6 mm			

- **Collar Pack Disassembly Incident**

During the disassembly of Collar pack #2, the coil support “spud” was not inserted into the RE bore before the side collar stacks were being removed. This caused an unsupported condition that resulted in the upper coils, Coils 3 and 104, to fall into the bore and onto the assembly table, respectively. See Figure 3.10. All the coils were inspected for any signs of damage, and while a few small areas were suspected, as evidenced by localized areas of cracked epoxy, these only appeared to be superficial in nature. Further tests showed that there were no electrical anomalies within the coil, although damage to the strain gauge wiring on Coils 05 and 104 had occurred. With this information, it was decided to continue with the assembly operations after repairs to the strain gauge wiring, as there were no other spare coils available at the time anyway.

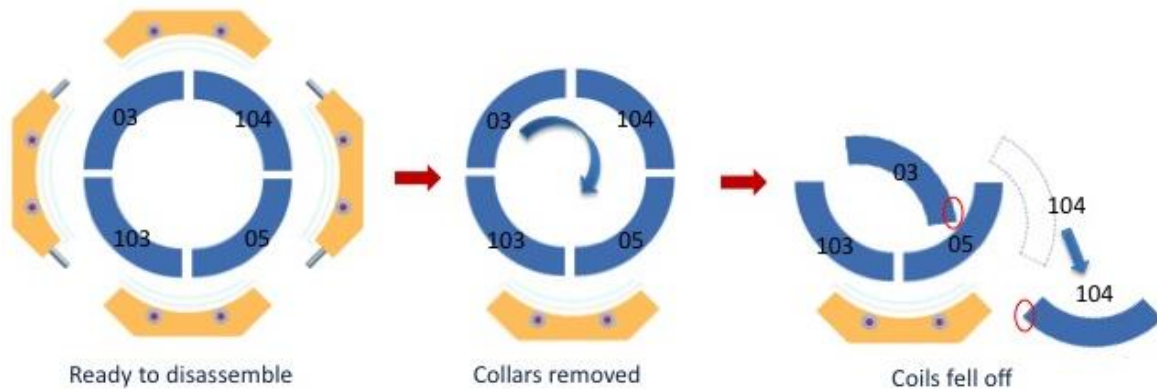


Fig. 3.10: Collar pack disassembly incident, as viewed from the Return End. Red circles indicate areas where coil impact was evident.

Assembly operations resumed after the repair work was completed, this time with redesigned support tooling and an updated disassembly procedure. The rest of the Collar pack assembly and disassembly processes resumed without further incident. A possibility of lower performance might be expected, though it remains to be seen during the magnet testing campaign. Reference [4] contains more details of the incident, as well as the findings and discussion.

#### d. Integration

- **Master Key Package Shims**

After the Coil pack (Collar pack plus the load pads) was assembled and torqued, mechanical measurements were taken of the Coil Pack size. Calculating the difference between these values and the measurements of yoke opening above determines the initial Master Key package shims. To ensure that all Master Keys start out the same size, the maximum value of the coil pack size is used with the minimum value of the yoke opening. The use of these numbers generates the maximum uniform Master Key Package size that can fit in all quadrants. Table 3.5 shows the values used and the amount of shims installed with the load keys.

Table 3.5: Maximum and minimums of the Coil Pack and Yoke opening. Calculated load key shim package to be uniform for all master keys.

	Coil pack, Max. size, in.	Yoke opening, min. size, in.	Total Min. difference, in.	Total Load Key thickness, in.	Initial Load key Shims, in.
Vertical	12.552"	15.166"	2.615"	0.517	0.043
Horizontal	12.550"	15.165"	2.614"		

Often in the insertion process, one master key package can be inserted as calculated, but the diametrically opposed master key requires fewer shims (e.g. a thinner package) in order to fit. Therefore, the bottom master key is always shimmed to the initial value and inserted before the insertion of the Coil pack, and the top master key is often inserted with a smaller shim package, for instance. See Fig 3.11. In the same way, one master key package on the side is also built to the calculated stack size and inserted, while the opposing side is assembled with a smaller shim package. Table 3.6 shows the shim package that was calculated, and the shim packages that were actually installed.

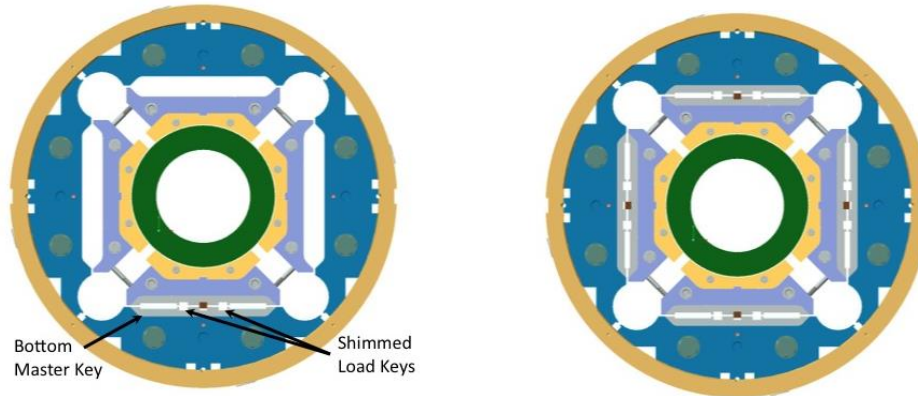


Fig. 3.11: (L) Bottom master key inserted into the assembly prior to installation of coil pack. (R) After insertion of all quadrants' master key packages. Both views from the LE shown.

Table 3.6: Initial load key shims inserted prior to the start of the magnet preload bladder operations.

<i>Viewed from the LE</i>	Top	Right	Bottom	Left
Initial load keys stack	0.492"	0.492"	0.515"	0.512"

- **Magnet Preload Operations**

The preload targets of the magnet are based on the limit of 200 MPa stress in the coil when cold. The 3-D ANSYS analysis shows that 200 MPa of stress is seen in the coil when the magnet is preloaded with 550 μm of interference at room temperature. As this is the first magnet of this family, a lower preload target of 475 μm interference was chosen, which is a typical approach used in the prior magnets in the past [5]. This corresponds to a 130 T/m gradient in the magnet. See Figure 3.12.

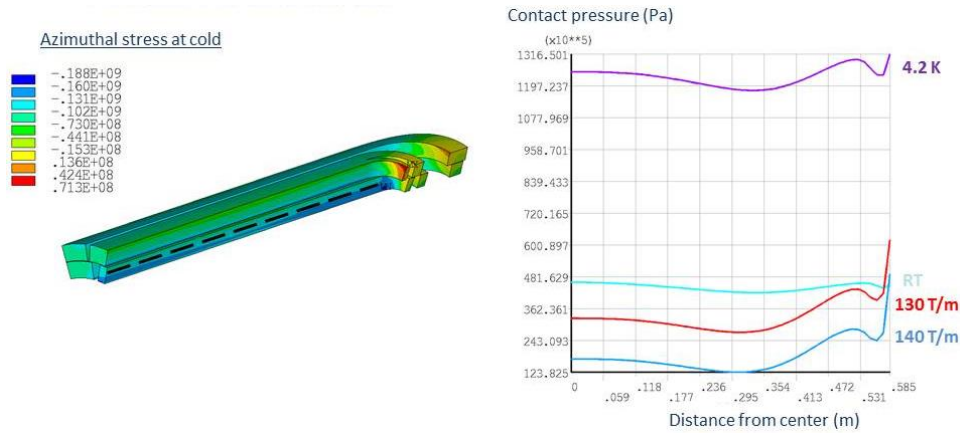


Fig. 3.12: ANSYS 3-D coil stress distribution for both 130 T/m and 140 T/m.

The first step in the bladder operations is to start with a uniform shim package on all the load keys. All quadrants were pressurized up to 1500 psi in order to maintain equal pressure all around, but we were unable to insert enough load shims into the Top and Right master keys to match that of the Bottom and Left master key packages. As this was the very first loading step, we chose not to go any higher to avoid potentially overstressing the coils. Therefore, individual quadrants were pressurized to a lower pressure (1000 psi) in order to start all packages at the same uniform stack size, but the initial bottom key stack was first reduced by 0.003”, and the new initial key stacks of 0.512” were inserted all around.

From this initial load key stack, we were able to insert 0.010” additional shims when all the bladder quadrants were pressurized at the same time at a maximum bladder pressure of 3500 psi. However, again, because there was concern about overstressing the coils during the preload operations, all subsequent load key increases were performed by pressurizing individual quadrants separately. See Table 3.7 for the shimming sequence and corresponding strain gauge readings.

Table 3.7: Load key shimming and strain measurements during the magnet preload operations. Values shown in grey indicate the yoke gap keys still in contact.

Bladder Pres. required, psi	Top, in.	Right., in.	Bot., in.	Left, in.	Avg. Coil $\mu\epsilon$	Avg. Shell $\mu\epsilon$
<i>Initial</i>	<i>0.492</i>	<i>0.492</i>	<i>0.515</i>	<i>0.512</i>	<i>-4 +/- 12</i>	<i>228 +/- 20</i>
1000 (single)	0.512	0.512	0.512	0.512	-30 +/- 32	354 +/- 21
2200 (all)	+0.005	+0.005	+0.005	+0.005	-103 +/- 37	543 +/- 24
3500 (all)	+0.010	+0.010	+0.010	+0.010	Values?	Values?
3000 (single)	+0.015	+0.015	+0.015	+0.015	Values?	Values
3500 (single)	+0.020	+0.020	+0.020	+0.020	-511 +/- 119	866 +/- 46
4200 (single)	+0.023	+0.023	+0.023	+0.023	-568 +/- 97	983 +/- 45
<i>Final Stack</i>	<i>0.538</i>					

A total of  $\sim 0.023''$  ( $\sim 580 \mu\text{m}$ ) key shims were inserted to achieve the target strain in the shell of  $960 \mu\epsilon$ . Even though the model dictated approximately  $475 \mu\text{m}$  of shim were required, we believe the  $\sim 100 \mu\text{m}$  extra is simply taking out the “fluff” of the coil pack assembly.

Figures 3.13 and 3.14 are the plots of the strain gauge data in the shells and coils during the operations, respectively, and Figure 3.15 is the transfer function expected from the ANSYS analysis.

After the azimuthal preload target was achieved, the next operation was the axial loading. The strain target of  $820 \mu\epsilon$  at room temperature for the rods corresponds to an axial tension of 169 MPa at 1.9 K; the value we achieved was  $820 \pm xx \mu\epsilon$ . This completed the preload operations of the magnet.

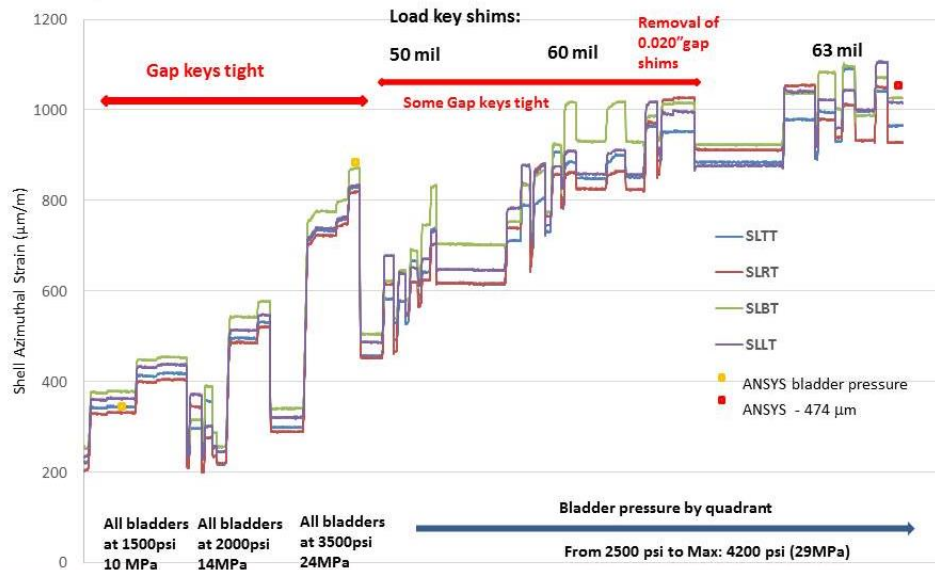


Fig. 3.13: Shell strain measurements, as a function of time during the bladder operations.

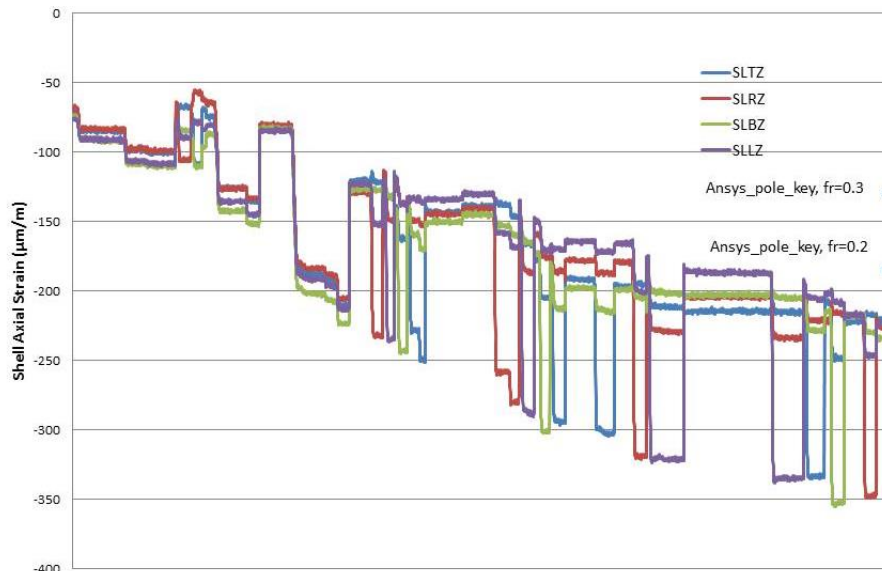


Fig. 3.14: Coil strain measurements, as a function of time during the bladder operations.

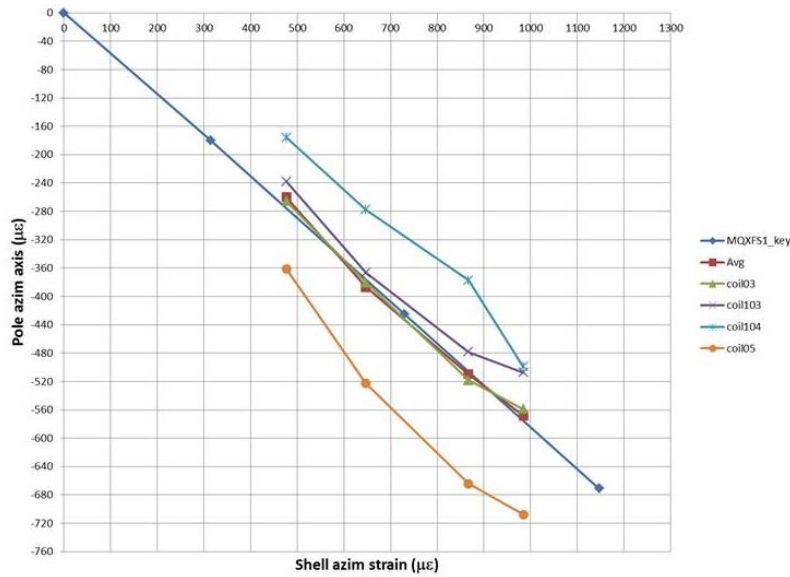


Fig 3.15: Magnet transfer function, as measured during the bladder preload operations.

- **Splice Connections**

The magnet splice connections were performed after the magnet preload operations were complete. Figure 3.16 (a) shows the physical layout of the magnet splice connections box, which is made up of two layers due to space constraints and the bend radius of the cables. Each of the leads was pre-tinned using Nokorode paste flux and SW SN62/Pb36/AG2 flat ribbon solder. Voltage taps measuring the leads (“CVT” and “FVT”) were also attached at this time for the purpose of monitoring the splice voltages when tested at the FNAL test facility. These VT wires are visible in Figure 3.16 (b).

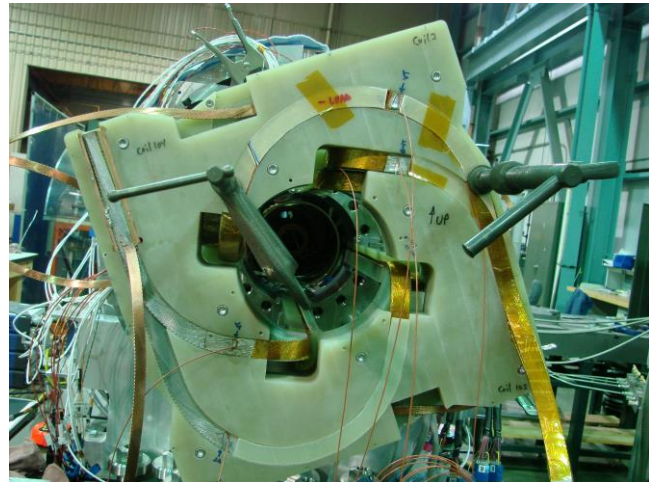
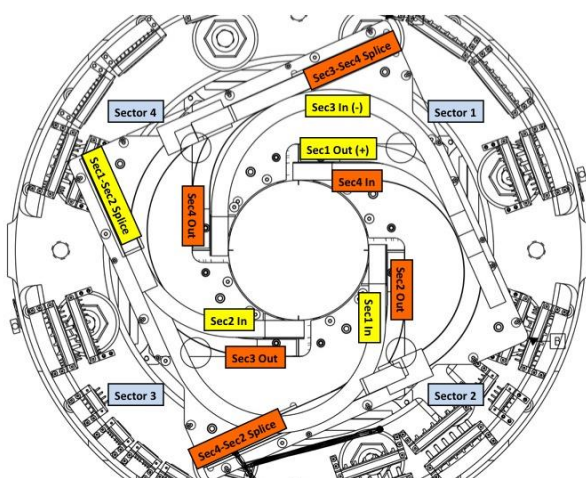


Fig. 3.16: (a) Diagram of the magnet splice connections. Orange labels represent leads on the first layer of the splice box; yellow labels represent leads on the second layer. (b) Splice operations on the second layer.

Voltage tap wires for VT01 also needed to be installed on the CERN coils (103 and 104) at the leads, as they were not installed at impregnation. Usually these tap wires are installed  $\sim 1$  cm from the end of the coil end shoe prior to impregnation, but because of the epoxy and insulation on the leads as received, a 5 cm offset from their usual location for these VTs was chosen. See Figure 3.17.

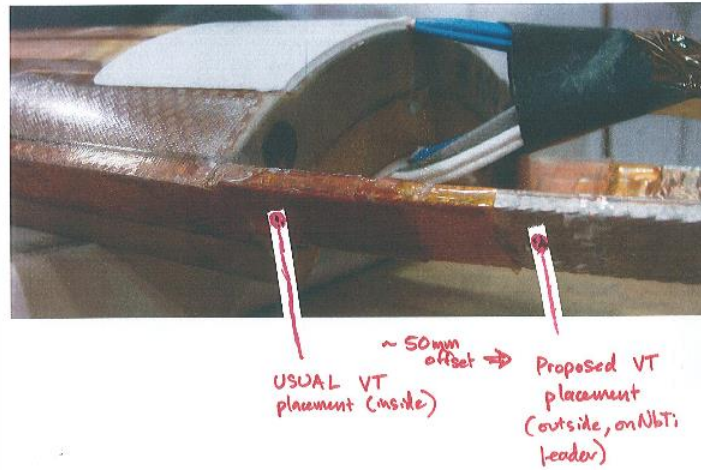


Fig 3.17: Location of the voltage tap VT01 on coils 103 and 104 (outer layer shown, also applies to inner layer).

- **Instrumentation Connectors**

Once the splice connection box was fully assembled, the connector skirts for the magnet were installed. These connector skirts were installed on both the Lead and Return Ends to capture the signals (VT, PH, and SG) exiting out from both ends. A RE-LE “pigtail” connects the signals from the RE to the distribution connectors on the LE; it passes through the cooling hole. More discussion on the instrumentation and connections is described below in the next section.

- **Packaging for shipment**

Finally, after the connectors have been installed and checked out, the magnet was packaged for shipment to FNAL.

## e. Instrumentation, Checkout and Magnet QC

- **Shell Strain Gauge Instrumentation**

Strain gauges were installed on Shell 1 in the center of the shell segment (azimuthal location was 387 mm from the end of the 774 mm long shell, per drawing 27H409. Each quadrant’s station was rotated  $15^\circ$  from both the horizontal and vertical planes. Initially, “LARP-style” (Vishay gauges) strain gauges were installed at the station, with the azimuthal gauge centered on the shell, and the axial gauge mounted 12.7 mm offset towards the return end. Each of these gauges was wired up in a full-bridge configuration with temperature compensators whose pads were fabricated from the same batch of Al7175-T74 material as the shells. All gauges were installed using the Vishay AE-10 bonding system, with a room temperature cure.

After the LARP-style gauges were installed, an additional set of “CERN-style” strain gauges (HBM type) was installed at each station, per the sketch shown in Figure 3.18. These were wired up in a half-bridge configuration with temperature compensators, and read with a different system (using AC excitation) from the LARP-style gauges. Again, these gauges were also bonded using the Vishay AE-10 bonding system. Table 3.8 lists the strain gauge types used, as well as their gauge factors.

Once the gauges were installed, the offsets were taken with the shell sitting on the bench in the horizontal orientation. This is considered the “zero”, or free-, state of the shell.

Table 3.8: Gauge factors for all gauges used.

	Shells	Coils	Rods
LARP (Vishay WK-13-125PC-350/W)	2.06	-	-
LARP (Vishay WK-05-125PC-350/W)	-	2.03	-
LARP (Vishay SK-13-120NB-350)	-	-	2.04
CERN (HBM 1-LC11-6/350)	2.22	-	-
CERN (HBM 1-XC11-3/350)	-	2.23	-

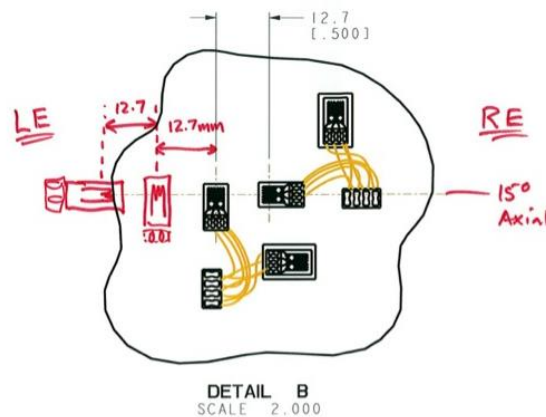


Fig. 3.18: Mounting location of the “CERN-style” HBM 1-LC11-6/350 quarter bridge strain gauges on the shell.

- **Coil Strain Gauge Instrumentation**

As with the shell, each of the four coils for this magnet was also instrumented with both styles of strain gauges. A single axial station at the center of the straight section of the coil was located 722 mm from the LE, which is the location of the centered LARP-style azimuthal gauge. The CERN-style gauge was installed 30 mm off the center toward the LE, with its azimuthal grid aligned to the centerline of the pole. See Figure 3.19. These gauges were all bonded using the Vishay AE-10 system.

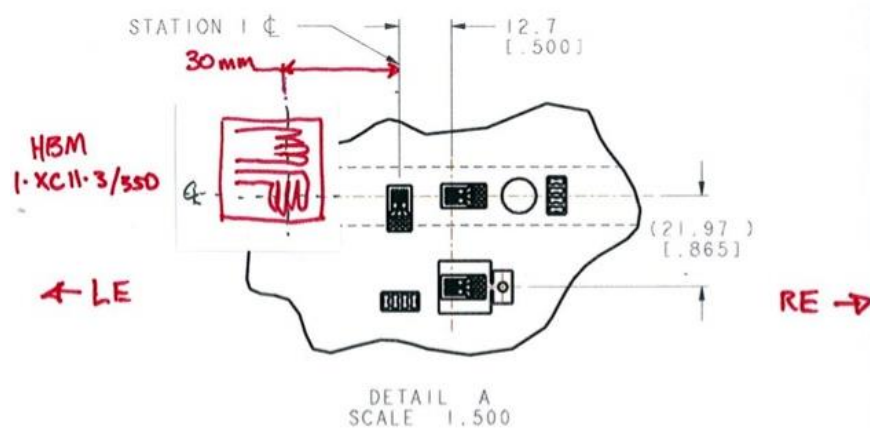


Fig. 3.19: Mounting location of the “CERN-style” HBM 1-XC11-3/350 half-bridge strain gauges on the coils.

After the instrumentation was installed the offsets were taken with the coils sitting on the bench in free state, and this is considered the “zero” state of the coils. It is commonly understood that the coils in this free state have a slight “banana shape”, which affects the early readings of the Collar pack and Coil pack assembly readings. As was seen in Table 3.7, the coil strain measurements at low pressures seem to exhibit this effect, showing a considerable spread in the low-pressure values.

- **Axial Rod Strain Gauge Instrumentation**

The strain gauges used for the axial rod differ from both the shell and coil implementations in that a full-bridge gauge foil was used; no external temperature compensation was employed, nor a second set of (HBM) gauges installed. Type SK-13-120NB-350 gauges were used, and the center of the gauge was mounted 195 mm from the LE of the rod, see Figure 3.20. After installation, the offsets were taken with the rods at rest on a table; the gauge factor for the gauges used is 2.04, as also seen in Table 3.8. When installed, the rods are rotated so that the strain gauges are facing outward radially from the bore.

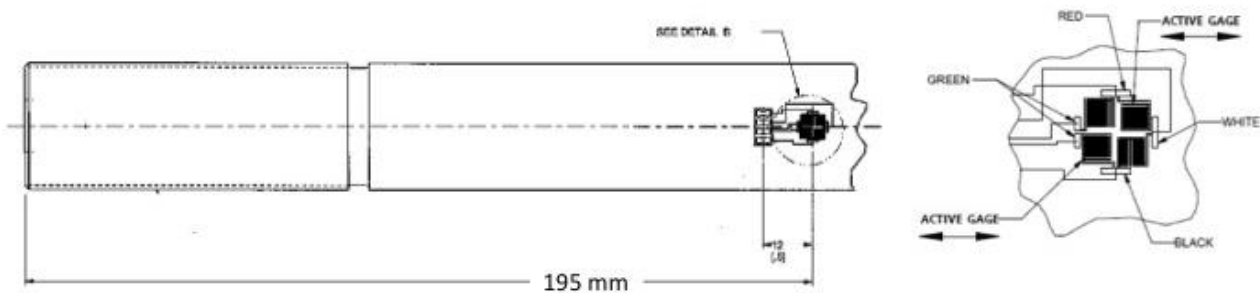


Fig. 3.20: Mounting location of the “LARP-style” only full-bridge strain gauges on the axial rods. LE is to the left.

- **Connector Skirts and Wiring**

The details of the MQXFS1 wiring connectors is detailed in [6].

All of the instrumentation (VT, PH, SG) from the magnet and coils were routed to connectors mounted to “skirts” located at both the LE and the RE of the magnet. The signals from the RE were only a few VT and PH channels, which were combined and routed to the LE via a wiring harness through one of the cooling holes in the magnet (“cooling hole pigtail”).

The LE connector skirt served several functions, collecting the SG, VT, and PH wires from each coil (both LE and RE), which were then distributed into connector module blocks that would interface with the wiring harness (“magnet pigtail”) to the Lambda plate at the FNAL test facility. See the Appendix for the wiring pinouts of each of these signals. Figure 3.21 shows images of the connector skirts.

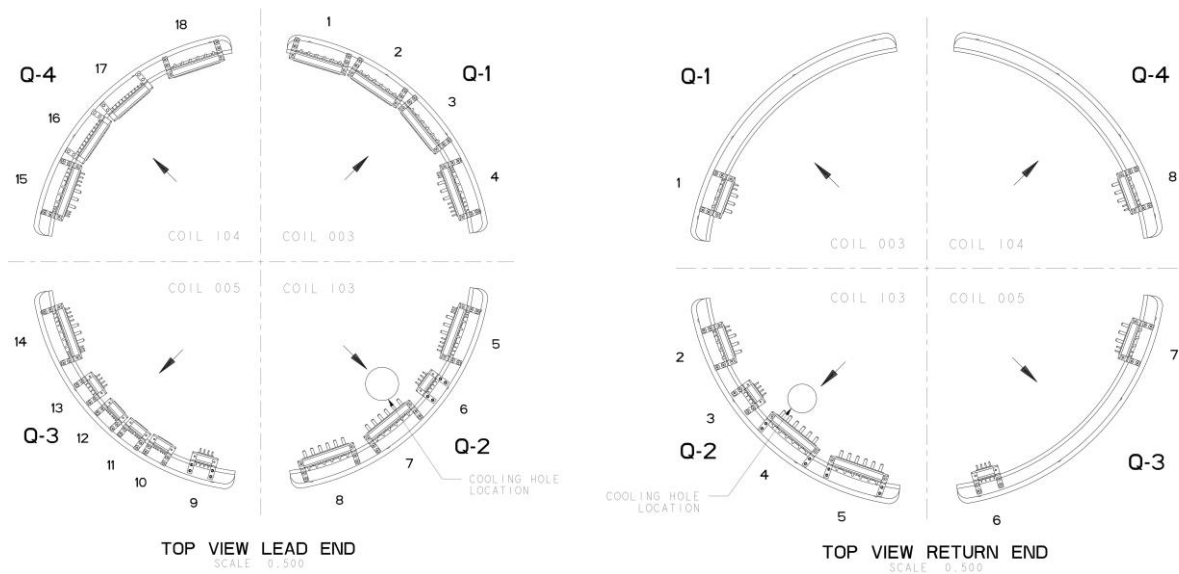


Fig. 3.21: Connector skirts connector layout.

- **Protection Heater Nomenclature and repair**

After the magnet wiring was completed, however, it we were made aware of a PH wiring naming convention error in the LARP coils (3 and 5). This was corrected by changing the jumpers wires at the RE skirts. See [7] for the details of the problem and the repair.

- **Magnet QC: Sequential R, Hipot, and Impulse Results**

Each coil was individually tested before the assembly of the magnet was started. There were no problems seen prior to the assembly. Additional information can be found in [ref]. After the magnet was assembled, QC tests on the completed MQXFS1 magnet were performed to ensure nothing damaged the electrical integrity of the coils during the process; these tests included sequential R, hi-pot, and impulse tests. The hipot and impulse values tested and passed are shown in Table 3.9. The impulse test plot is shown in Figure 3.22, which was performed at 500 V, 1000 V, 1500 V, and then 200 V steps from 1600 to 2000. The Sequential R plot is shown in Figure 3.23. Again, no anomalies were observed.

Table 3.9: Tests performed on the MQXFS1 magnet before shipping. All hipot tests ramp rate was 5 V/sec.

	Value, V	Passed	Notes
Coil to Structure (heater floating)	2500		$\leq 2.6 \mu\text{A}$
Coil to Protection Heaters (structure floating)	2500		$\leq 3.0 \mu\text{A}$
Protection Heaters to Structure (coil floating)	2500		$\leq 0.4 \mu\text{A}$
Impulse tests (up to)	2000		
PVT, FVT Pigtail Cables (pins to braided shield)	2500		$\leq 0.2 \mu\text{A}$

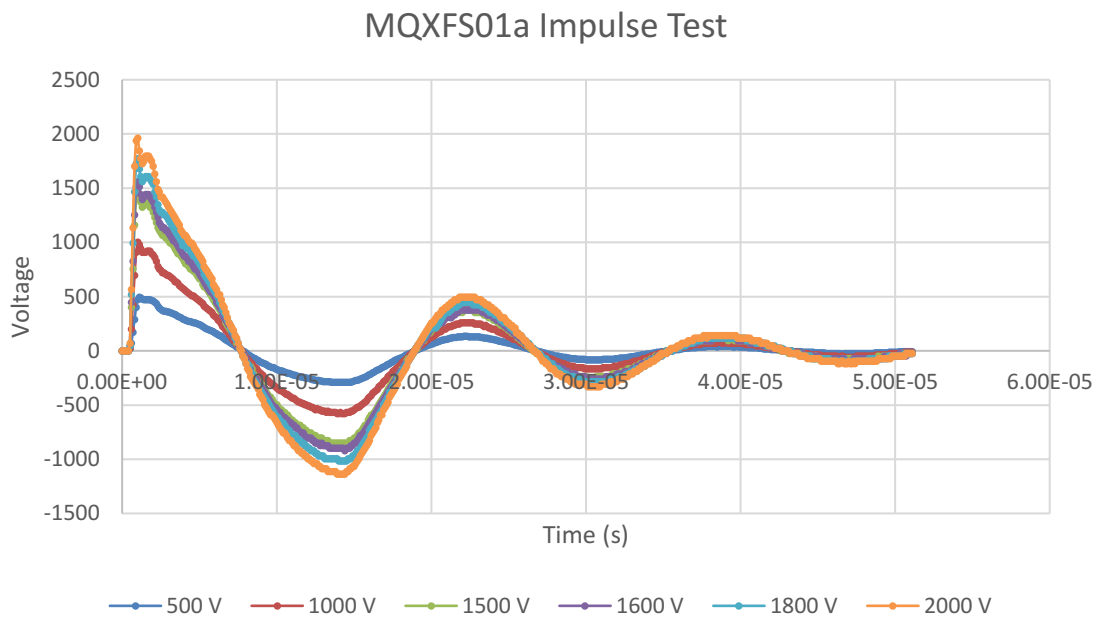


Fig. 3.22: Impulse test plots for the MQXFS1 magnet.

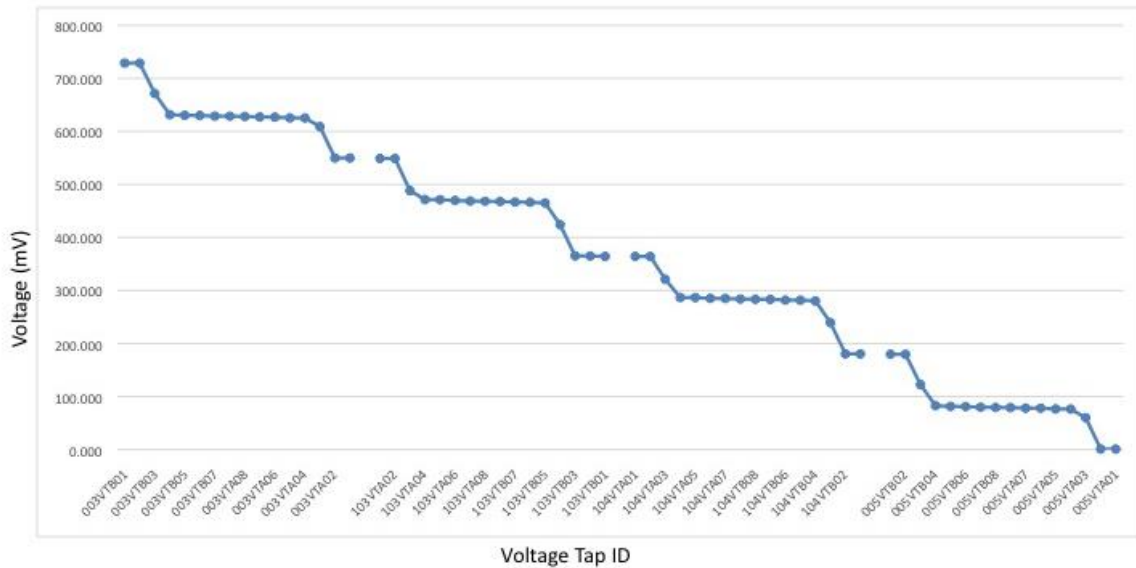


Fig. 3.23: Sequential R measurements of MQXFS1.

- **Magnet QC: Strain gauge wiring**

While each of the components—skirt connectors, pigtails, etc.—were all verified as valid connections at the assembly, it was noted that the primary magnet pigtail seemed to be particularly sensitive to broken wires at the SG connectors. These were repaired before packaging for shipment, but not necessarily guaranteed to withstand a thermal cycle.

## References

- [1] G. Ambrosio, P. Ferracin, et al., “MQXFS1 Design Report” (<http://larpdocs.fnal.gov//LARP-public/DocDB/ShowDocument?docid=1074>).
- [2] Plone [link  
http://plone.uslarp.org/MagnetRD/qxf/meetings/2015/20150408structureWG/2015\\_04\\_08\\_MQXFS\\_D\\_assembly\\_summary.pptx](http://plone.uslarp.org/MagnetRD/qxf/meetings/2015/20150408structureWG/2015_04_08_MQXFS_D_assembly_summary.pptx)
- [3] Plone [link  
http://plone.uslarp.org/MagnetRD/qxf/meetings/2015/20150624structurecoilWG/2015\\_06\\_23\\_MQXFS1\\_radial\\_shim\\_proposal.pptx](http://plone.uslarp.org/MagnetRD/qxf/meetings/2015/20150624structurecoilWG/2015_06_23_MQXFS1_radial_shim_proposal.pptx)
- [4] Indico Meeting Notes and discussion  
<https://indico.fnal.gov/conferenceDisplay.py?confId=10192>
- [5] Indico Meeting Notes:  
<https://indico.fnal.gov/conferenceDisplay.py?confId=10283>
- [6] “MQXFS1 Wiring connectors”, X. Wang, November 19, 2015.
- [7] “MQXFS1 OL heater strip connections in coils #3 and #5”; G. Chlachidze, Jan 28.2016.

## 4. QUENCH PROTECTION

This model magnet is equipped with quench heater strips and with CLIQ terminals. Dedicated experimental studies are foreseen, aimed at demonstrating the quench protection of the MQXF magnets in the LHC tunnel and at assessing the performance of different types of quench heater strips, of alternative CLIQ configurations, and of combinations of these.

### a. Quench heater strips

Six quench heater strips were attached to each pole:

- Two strips to the inner layer (A01, A02)
- Two strips to the outer layer in the mid-plane low-field region (B01, B04)
- Two strips to the outer layer in the high-field region (B02, B03)

Different types of strips were attached to poles manufactured by CERN and by LARP. The designs chosen for the strips of each pole are listed in Table X1, with reference to the naming used in the MQXFS1 design report [1] and in [2]. The position of the heater strips is schematized in Fig. 4.1. Note that the strips of each pole are numbered starting from the strip closest to the lead end.

Table 4.1: Design implemented for the quench heater strips of the MQXFS1 magnet

Pole	Sector	Coil ID	Inner Quench heaters	Outer Quench heaters
Q-1	D	3	Copper-plated heater design 1	Stainless steel-only design
Q-2	C	104	Copper-plated heater design 2 IL	Copper-plated heater design 2 OL
Q-3	B	5	Copper-plated heater design 1	Stainless steel-only design
Q-4	A	103	Copper-plated heater design 2 IL	Copper-plated heater design 2 OL

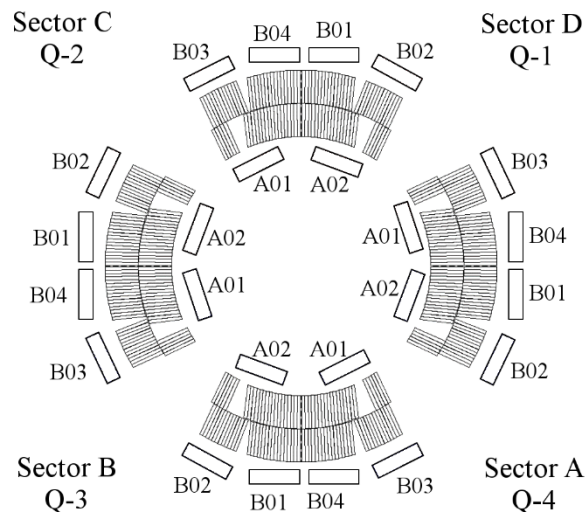


Fig. 4.1: Position of the heater strips attached to the MQXFS1 magnet, viewed from the lead side. The adopted naming system is the same proposed in [2].

The main parameters of the four types of heater strips and their estimated resistances at cryogenic and room temperature are summarized in Table 4.2 [1]. For the resistance calculations, the applied magnetic field is considered nihil, the resistivity of stainless steel is assumed to be  $5.00E-7$  and  $6.67E-7$   $\Omega\text{m}$  at 10 and 293 K, respectively (RRR=1.33), and that of copper  $6.54E-9$  and  $1.75E-8$   $\Omega\text{m}$ , respectively (RRR=26).

The values of the quench heater strips measured at cryogenic and at room temperature, in absence of applied magnetic field, including the resistance of the copper leads connected to the strips, are listed in Tables 4.3 and 4.4, respectively.

In Tables 4.5 and 4.6, for each different design the measured strip resistances are compared to the design values at cryogenic and room temperature, respectively.

Table 4.2: Parameters of the quench heater strips attached to the MQXFS1 magnet [1]

	Cu-plated 1 IL	SS-only OL	Cu-plated 2 IL	Cu-plated 2 OL*
Strip length [m]	1	1	1	1
Heater SS width [mm]	10		20	20
Heater Cu width [mm]	9.4	-	5	20
Heater SS thickness [mm]	0.025	0.025	0.025	0.025
Heater Cu thickness [mm]	0.01	-	0.01	0.01
Station length [mm]	18.3		25	40
Station period [mm]	91		65	160
Number of stations	20	16	19	8-9
Strip resistance @ 10 K [ $\Omega$ ]	0.83	1.43	0.57	0.35-0.40
Strip resistance @ 293 K [ $\Omega$ ]	1.25	1.91	0.90	0.51-0.57
*Note: Heater strips featuring a “Cu-plated 2 OL” design have 8 or 9 heating stations when located in the high- or low-field region of the coil, respectively.				

Table 4.3: Measured cryogenic-temperature resistances of the heater strips attached to the MQXFS1 magnet, including copper leads connected to the strips

	Coil 3	Coil 104	Coil 5	Coil 103
A01 (Inner, R)	0.794	0.520	0.783	0.512
A02 (Inner, L)	0.855	0.524	0.821	0.515
B02+B03 (High-field, L+R)	4.64	0.693	4.45	0.695
B01+B04 (Low-field, L+R)	4.37	0.782	4.36	0.78
Note: The resistances of the heater strips attached to the outer layer of the magnet were measured in pairs, connecting in series two high-field or low-field strips.				

Table 4.4: Measured room-temperature resistances of the heater strips attached to the MQXFS1 magnet, including copper leads connected to the strips

	Coil 3	Coil 104	Coil 5	Coil 103
A01 (Inner, R)	1.37	0.9748	1.379	0.9318
A02 (Inner, L)	1.42	0.9667	1.386	0.9285
B01 (Low-field, L)	3.23	0.6621	3.132	0.6481
B02 (High-field, L)	3.21	0.6157	3.123	0.5995
B03 (High-field, R)	3.27	0.6215	3.182	0.6076
B04 (Low-field, R)	3.31	0.6692	3.195	0.6551

Table 4.5: Comparison between design and measured cryogenic-temperature resistances of the heater strips attached to the MQXFS1 magnet, including copper leads connected to the strips

	Cu-plated 1 IL	SS-only OL	Cu-plated 2 IL	Cu-plated 2 OL	
Design resistance [ $\Omega$ ]	<b>0.83</b>	<b>1.43</b>	<b>0.57</b>	<b>0.35</b>	<b>0.40</b>
Average measured resistance [ $\Omega$ ]	0.813	2.228	0.518	0.347	0.391
Max measured resistance [ $\Omega$ ]	0.855	2.320	0.524	0.348	0.391
Min measured resistance [ $\Omega$ ]	0.783	2.180	0.512	0.347	0.390

Table 4.6: Comparison between design and measured room-temperature resistances of the heater strips attached to the MQXFS1 magnet, including copper leads connected to the strips

	Cu-plated 1 IL	SS-only OL	Cu-plated 2 IL	Cu-plated 2 OL	
Design resistance [ $\Omega$ ]	<b>1.25</b>	<b>1.91</b>	<b>0.90</b>	<b>0.51</b>	<b>0.57</b>
Average measured resistance [ $\Omega$ ]	1.389	3.207	0.950	0.611	0.659
Max measured resistance [ $\Omega$ ]	1.420	3.310	0.975	0.622	0.669
Min measured resistance [ $\Omega$ ]	1.370	3.123	0.929	0.600	0.648

The nominal heater connection scheme for this model magnet is as follows:

- Strip A01 of each pole are powered alone
- Strip A02 of each pole are powered alone
- Strips B01 and B04 of the same pole are connected in series and powered together
- Strips B02 and B03 of the same pole are connected in series and powered together

## b. CLIQ terminals and leads

Three CLIQ leads are attached to the magnet, each located at the joint between two electrically connected poles (see taps a, b, c shown in Fig. 4.2 (a)). Their terminals are connected at the coil ends in the “pizza box”. The electrical order of the four poles is as follows: Q-1, Q-2, Q-4, Q-3.

The parameters of the conductor used for the CLIQ leads are summarized in Table 4.7. Before a CLIQ discharge, the leads are in the superconducting state. It is difficult to predict whether the leads will be quenched or not during the current oscillations introduced by the CLIQ system, due to the complex magnetic transients occurring at the coil ends. Hence, the copper cross-section of the leads is dimensioned to avoid overheating during the CLIQ discharge and to not limit the CLIQ performance due to an excessive electrical resistance. The temperature in the leads is expected to remain well below 300 K even if it turned resistive right at the beginning of the CLIQ discharge.

Table 4.7: Parameters of the conductor used for the CLIQ leads of the MQXFS1 magnet

Parameter	Value
Conductor type	Nb-Ti cable
Cable No.	L7I-B00985
Conductor dimensions [mm]	10.0 x 1.3
Fraction of copper	

The three terminals allow flexibility in the choice of the CLIQ configuration. Three configurations are particularly interesting and will be tested to assess their performance and validate the models [3-5]:

- 1-CLIQ Crossed-Poles, obtained by introducing opposite current changes in poles which are physically adjacent (see Fig. 4.2 (a)); this is the baseline configuration for the protection of the full-scale magnet [6];
- 1-CLIQ Upper-Lower-Poles, obtained by introducing opposite current changes in the two upper and in the two lower poles (see Fig. 4.2 (b)); this configuration is less efficient;
- 2-CLIQ Crossed-Poles, obtained connecting two individual units (see Fig. 4.2 (c)).

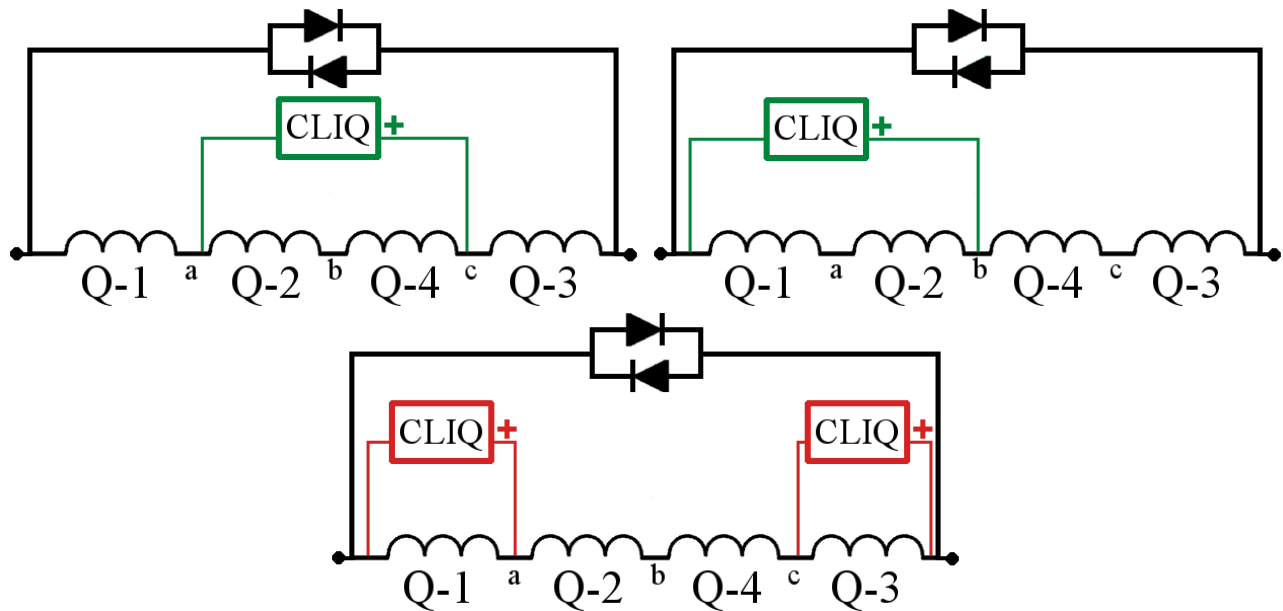


Fig. 4.2: Position of the CLIQ terminals and proposed CLIQ configurations: 1-CLIQ Crossed-Poles (a, Top left scheme), 1-CLIQ Upper-Lower-Poles (b, Top right scheme), 2-CLIQ Crossed-Poles (c, Bottom scheme).

## References

- [1] G. Ambrosio, P. Ferracin, et al., “MQXFS1 Design Report” (<http://larpdocs.fnal.gov//LARP-public/DocDB/ShowDocument?docid=1074>).
- [2] J. DiMarco, GL. Sabbi, and X. Wang, “Coordinate system for magnetic measurements of MQXF magnet”, LARP note, 2015.
- [3] E. Ravaioli, “CLIQ”, PhD thesis University of Twente, The Netherlands, 2015, doi: 10.3990/1.9789036539081.
- [4] E. Ravaioli et al., “New, Coupling Loss Induced, Quench Protection System for Superconducting Accelerator Magnets”, IEEE Trans. Appl. Supercond., vol. 24, no. 3, June 2014, doi: 10.1109/TASC.2013.2281223.
- [5] E. Ravaioli et al., “Protecting a Full-Scale Nb3Sn Magnet with CLIQ, the New Coupling-Loss Induced Quench System”, IEEE Trans. Appl. Supercond., vol. 25, no. 3, June 2015, doi: 10.1109/TASC.2014.2364892.
- [6] E. Ravaioli et al., “Advanced Quench Protection for the Nb3Sn Quadrupoles for the High Luminosity LHC”, IEEE Trans. Appl. Supercond., 2016.